Quantum Networks Using Rare-Earth Ions

Rare-earth ion-doped crystals are key for quantum networks, acting as photon sources, optical quantum memories, and qubits due to their long spin coherence, enabling on-chip integration with nanophotonics (like cavities) for efficient light-matter interfaces, crucial for quantum repeaters, with recent advances focusing on spectral tailoring, hybrid systems (quantum dots + memories), and molecular crystals for new platforms, pushing towards scalable quantum internet nodes with high fidelity. Shown concepts and recent work related to creating their unique suitability for creating photon sources, optical quantum memories for light, and qubits that allow quantum information processing.

1. Introduction

The increasing possibility to control nature at a scale where quantum effects arise creates opportunities that could only be dreamed of a few years ago. It has allowed understanding some of the most counter-intuitive predictions of quantum theory such as entanglement, distant particles whose properties are tied together[1][2][3][4][5][6][7]. In turn, this has spurred a world-wide race to create the quantum internet[8]. This revolutionary network promises provable-secure communication using quantum key distribution (QKD)[9], networked[10] and blind quantum computing[11], and distributed quantum sensing[12]. Common to all is the need for light–matter interfaces that employ atoms or optically addressable centres[13][14][15], ideally in the solid-state environment. For instance, single emitters allow the creation of single photons and multi-photon entangled states[16][17][18][19] as well as spin–photon and spin–spin entanglement[7][20][21]; a collection of interacting centres enables quantum gates for quantum information processing[22]; and large ensembles can be used for photon-multiplexed quantum memory (QM)[23], which is key to quantum repeaters and hence long-distance quantum communication[24][25]. For compatibility and scalability, these components should ideally be based on the same type of defect and be on-chip integrable using standard photonics technology.

Due to their unique combination of suitable energy levels with long lifetimes, large inhomogeneous broadening, and remarkable optical and spin coherence times, ensembles of rare-earth ions doped into inorganic crystals have emerged during the past decade as excellent choices for optical QMs[26]. In addition, their long spin coherence times, up to hours in the case of Eu:Y_2SiO_5[27], make them highly suitable for encoding long-lived qubits, enabling the creation of spin–photon or spin–spin entangled states[28][29]. Furthermore, the possibility for controlled dipole–dipole interactions underpins their potential for multi-qubit quantum information processing[30]. However, the long excited-state lifetimes of rare-earth ions, a prerequisite for the long optical coherence time needed for multiplexed QMs, also represent a caveat as they hamper the observation of spontaneous emission from individual ions. This impacts the observation of single photons, and, by extension, the creation of entangled states and of optical readout of individual qubits. This problem can be solved by exploiting the Purcell effect, which allows increasing the ions' emission rate by coupling it to a mode of a nano- or micro-cavity[31][32][33][34][35][36][37][38][39][40] (see[41] for an alternative approach). In turn, this opens the path toward the creation of compatible and on-chip integratable single-photon emitters, individual ion QM for light, and long-lived qubits based on the same material platform.

This review is organized as follows. First,there is a general introduction to quantum networks and quantum repeater architectures whose developments are currently pursued by many groups worldwide. Next,a brief discussion of the properties of rare-earth ions that underpin their potential as light–matter interfaces for future quantum networks. Sections 4–6 describe three different use cases: single-photon sources, QM for light, and single qubits that allow quantum information processing. In section 7, a review recent work towards elementary quantum repeater links. Finally, an outlook with a brief discussion of remaining challenges and future research directions in section 8.

The figure below shows the sample transparent nanophase glass ceramics with nanocrystals of zinc oxide and erbium ions. The sample is excited by radiation of a UV laser. The beam of laser radiation experiences multiple total internal reflection. Yellow and green luminescence is connected with nanocrystals of ZnO and ions Er3+, respectively. Because of the heterogeneity of the glass-ceramic due to the influence of rare earth ions on its crystallization, the color of the luminescence changes as the propagation of laser radiation.

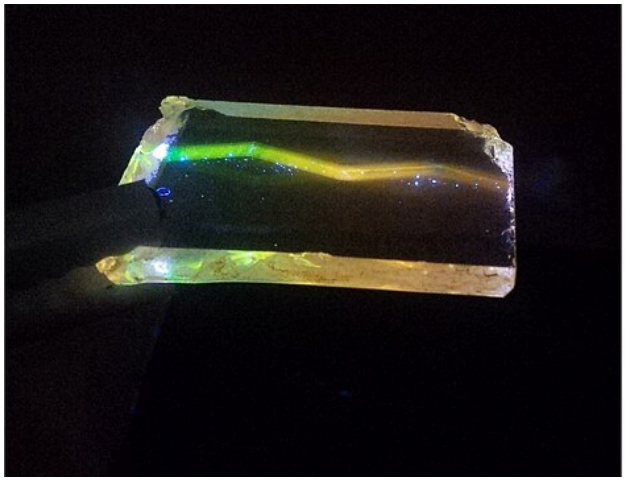

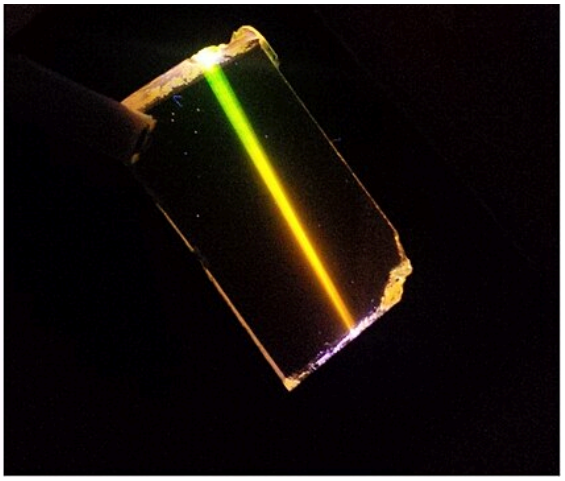

2. Quantum repeaters and quantum networks

2.1. Quantum networks

For this article a quantum network consists of **network nodes** that allow the execution of quantum applications, and **photonic communication links** that enable the exchange of quantum information across fibre and free-space (including satellite-based) quantum channels. To compensate for transmission loss, these links may use quantum repeaters and include **quantum repeater nodes** and **quantum link nodes**.

While some basic benefits can already be retrieved from quantum networks composed of network nodes that can only emit attenuated laser pulses and perform single qubit projection measurements, QKD over trusted nodes is a well-known example[42][43][44][45][46], here assume fully quantum-enabled nodes that can emit quantum states of light, contain one or several long-lived qubits, and allow single and multi-qubit unitary operations (gates) and measurements. These nodes are connected through fibre or free-space channels into a small, e.g. metropolitan area quantum network, and allow executing general quantum network applications. Network nodes may also be connected to **quantum link nodes** that allow quantum communication with other, distant, network nodes through chains of **quantum repeater nodes** and additional **quantum link nodes**. Finally, to span long distances, e.g. inter-continental distances, imagine connections to and between satellites that may relay quantum information using direct optical links, repeater-based links, or even by physically transporting stored quantum information from one place to another. The cartoon in figure 1 shows a generic example of such a network. Note that some nodes may play more than one role, e.g. quantum networks nodes may double as quantum repeater nodes or link nodes.

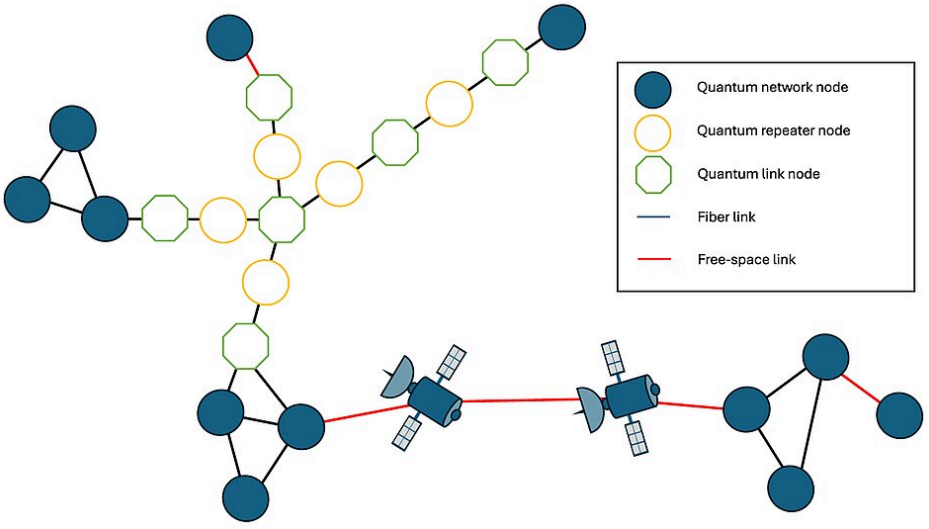

Fig.1. Quantum network. Illustration of a generic quantum network composed of network nodes, repeater nodes, link nodes, and fibre- as well as free-space (including satellite-based) photonic links.

perfectly, correlated measurement results of particles that can in principle be arbitrarily far away. As such, entanglement is a fundamental resource empowering future quantum networks, allowing, e.g. provable-secure establishment of cryptographic keys by means of QKD[9] and the faithful transfer of an unknown quantum state between distant nodes using quantum teleportation[49]. Unfortunately, photons, the particle of choice to distribute entanglement, are subject to loss and decoherence as they travel through optical fibres, limiting the extension of quantum networks of the type described above to around 100 km. Solutions to this problem are quantum repeaters[24][50], the transmission of entangled photons to distant locations using satellites instead of fibres[51], or a combination thereof.

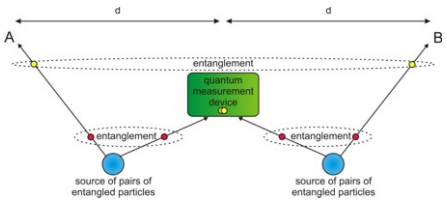

Entanglement

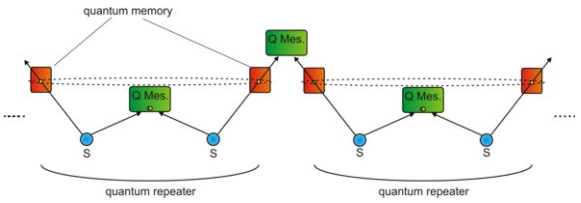

Long range repeating

Figures 2 and 3 illustrate two different approaches to quantum repeaters. The first takes advantage of entanglement creation across **elementary links,** the basic building block of a repeater-based quantum communication link, using highly multiplexed (ensemble-based) QMs and equivalently multiplexed photon-pair sources[52], making them nearly deterministic. It furthermore employs entanglement connection (entanglement swapping) between neighbouring elementary links using linear-optics Bell state-measurements[53]. This measurement is generally assumed to be probabilistic[47], but note that it can in principle be achieved deterministically by adding auxiliary entangled photons[54][55]. The second approach is based on the probabilistic creation of entanglement across elementary links using individual ions as qubits and single photons, and Bell-state measurements to connect adjacent links based on the deterministic interaction between two neighbouring rare-earth ions[56]. Using many qubits, this architecture also offers the possibility for multiplexing, however, at a smaller degree than the first approach. Note that it is in principle possible to combine the best of both worlds[57], however, here the focus is on architectures that are already under experimental development using rare-earth ions. But regardless of the approach, all these approaches derive their improved scaling compared to entanglement distribution without quantum repeaters from the possibility of connecting elementary links **after** confirmation of entanglement distribution.

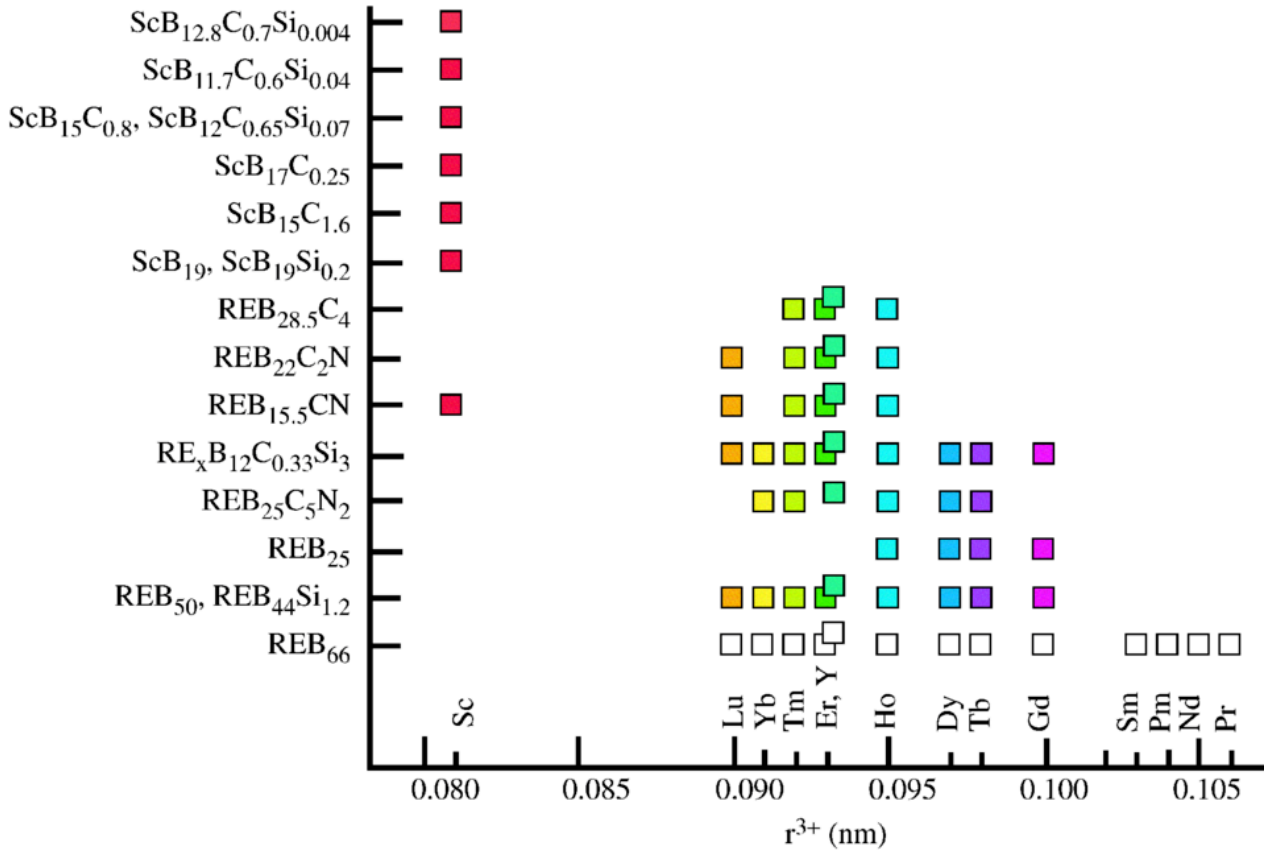

The image is a scientific plot from materials science literature on metal borides, specifically scandium borides and rare earth borides (RE borides, where RE stands for rare earth elements).

Overall Structure

- - **X-axis**: Labeled "r^{3+} (nm)", representing the trivalent ionic radius of the metal cation in nanometers, ranging from ~0.080 to ~0.105 nm.
- - **Element labels** along the x-axis (from left/smallest radius to right/largest radius):**Sc**, **Y**, **Lu**, **Tm**, **Er**, **Ho**, **Dy**, **Tb**, **Gd**, **Eu**, **Sm**, **Nd**, **Pr**, **Ce**, **La**.
- **Y-axis**: Lists various boride compound compositions (no numerical scale; the vertical order reflects a trend from lower to higher boron content or structural complexity downward).
- - **Data representation**: Each compound has one or more colored square markers placed horizontally at the x-position corresponding to the ionic radius of the metal(s) for which that phase has been reported/synthesized. The squares indicate known stable compositions for specific cations.

Detailed List of Compounds and Markers (top to bottom)

1. $ScB_{12.8}C_{0.7}Si_{0.004}$ Single maroon/red square at the Sc position (leftmost).
2. $ScB_{11.7}C_{0.6}Si_{0.04}$ Single red square at Sc.
3. $ScB_{15}C_{0.8}$, $ScB_{12}C_{0.65}Si_{0.07}$ (two related compositions listed together) Single red square at Sc.
4. $ScB_{17}C_{0.25}$ Single red square at Sc.
5. $ScB_{15}C_{1.6}$ Single red square at Sc.
6. ScB_{19}, $ScB_{19}Si_{0.2}$ Single red square at Sc.
7. $REB_{28.5}C_4$ Three colored squares (yellow, lime green, cyan) at mid-small radii.
8. $REB_{22}C_2N$ Four colored squares (orange, yellow, green, cyan).
9. $REB_{15.5}CN$ Five colored squares (red + orange, yellow, green, cyan).
10. $RE_xB_{12}C_{0.33}Si_3$ Six colored squares (orange, yellow, green, cyan, blue, magenta), spanning a wider range of mid radii.
11. $REB_{25}C_5N_2$ Five colored squares (yellow, green, cyan, blue, magenta).
12. REB_{25} Three colored squares (cyan, blue, magenta).

Key Trends and Interpretation

Size effect: The plot demonstrates a strong dependence of boride phase stability on cation size.

- - Smallest cation (Sc^{3+}) only forms higher borides when stabilized by small amounts of carbon (C) and/or silicon (Si) substitution. Pure Sc borides without C/Si are not shown in higher stoichiometries.
- - As ionic radius increases (moving right), progressively boron-richer phases become stable, often still requiring C, N, or Si in intermediate cases.
- - Largest cations (Ce^{3+}, La^{3+}) can stabilize extremely boron-rich phases like REB_{66} without additional elements.

Color coding: The rainbow progression (red → orange → yellow → green → cyan → blue → magenta) appears to simply distinguish different rare earth elements, with each color corresponding to a specific RE at its ionic radius position. Red is used exclusively for Sc phases. White open squares for REB_{66} likely indicate the phase is known for many (or potentially all) large RE ions.

- **Structural implication**: Higher borides have complex boron frameworks ($e.g., B_{12}$ icosahedra clusters). Larger cations better fit the structural voids, allowing higher boron content without needing C/Si to ``prop up *the lattice.*

This type of figure is common in reviews of rare earth and actinide higher borides, illustrating why scandium borides require heteroatoms (C/Si) for high boron content while large rare earths like lanthanum do not. The plot summarizes experimental reports of synthesized phases across the series.

The rare-earth elements are characterized by partially filled 4f shells. When doped into inorganic crystals, they generally form trivalent (triply positively charged) ions with inhomogeneously broadened 4f–4f transitions in the visible and near-infrared, with excited state lifetimes (T_1) that often exceed 1 ms. The crystal field interaction lifts the degeneracy of the electronic states given by $2S+1L_J$ (where $2S+1, L, J$ are, in this order, the spin multiplicity, the angular momentum and the total angular momentum). Depending on whether the ion has an even (non-Kramers ion) or odd (Kramers ion) number of electrons, this results in $2J+1$ or $(2J+1)/2$ crystal field levels (or Stark levels) with effective electron spin $S=0$ and $S=1$, respectively. The optical transition of interest typically couples the lowest crystal field levels of each electronic state, $Z_0 \rightarrow Y_0$, a so-called zero-phonon line (ZPL). The Z_0 (Y_0) level has a Zeeman/hyperfine structure that depends on the electron spin S and the nuclear spin I, resulting in a rich diversity of possible hyperfine manifolds according to the rare-earth element, its specific isotope, and the point symmetry of the doping site in the crystal.

At cryogenic temperatures < 4 K, optical coherence times (T_2) of the optical ZPLs can approach T_1, and for some cases they exceed 1 ms[64][65][66]. This feature distinguishes rare-earth ions from all other solid-state emitters. Similarly, population lifetimes T_1 and coherence times T_2 between hyperfine levels within Z_0 manifold can be very long, with T_1 values of weeks[67][68] and T_2 values of hours[27] having been reported, respectively. For an introduction to the properties of rare-earth ion-doped crystals at cryogenic temperatures, see[48][69][70][71].

4. Network components: single and entangled photons

4.1. Spontaneous parametric down-conversion (SPDC)

The current push by many countries to establish extended quantum networks is based on thorough understanding of its constituents and their interplay, as well as on a large number of proof-of-principle demonstrations of ever-increasing complexity by us and others. At the heart of this development have been sources of photon pairs based on SPDC, a process in which a strong pulse of light, the pump, is probabilistically converted inside a non-linear crystal into a pair of entangled photons, first demonstrated in 1970[72]. SPDC sources have rapidly gained a lot of attention both for fundamental tests of nature[4][5][73][74][75] as well as for applications such as QKD[76][77][78] and quantum teleportation[79][80], including deployed over optical fibres[81][82], over free-space links between optical ground stations[83], and even to a satellite[84].

However, the state created by SPDC sources is not a true two-photon state, but rather a two-mode squeezed state, characterized by an even number of emitted photons. In qubit-based quantum communications one generally only considers the case with two photons (one pair), which describes the desired state $|\psi\rangle = \frac{1}{\sqrt{2}}(|01\rangle - |10\rangle)$. But the undesired higher-order contributions also exist, and it is unavoidable that 4 or 6 photons will sometimes be emitted. This problem is often countered by reducing the pump power so that the

inefficient in the case in which the Bell state measurements are based on the detection of a single photon. Worse, in case the projection onto a Bell state is indicated by the detection of two photons, it is not suitable at all[85]. Indeed, the best connection between two distant QKD nodes then uses only a single elementary link, concatenation of several links is not useful, and the repeaterless bound[86], a fundamental bound that describes the scaling of the secret key rate as a function of loss assuming no quantum repeater, cannot be violated (see[87] for an early version).

It is therefore important to develop better sources of entangled photons, a task that is further complicated by the need for spectral compatibility with optical QMs and telecommunication fibres. Several approaches have been proposed and/or implemented, including post selection of desired SPDC emissions[88][89][90], suppression of undesired emissions[91]; the use of individual emitters[92][93]; and fusion of four (non-entangled) single photons, also created using individual emitters, into one heralded pair[18][94]. Motivated by the latter, focus in the following on the creation of single photons.

4.2. Cavity-enhanced single photon emission

True single photons are highly valuable resources for quantum communication protocols such as QKD[9], but also for different quantum repeater architectures[25], including as a resource for heralded entangled photon pairs[18][94]. They have been created using several types of solid-state emitters such as quantum dots[16][17], diamond vacancy centres[95][96] and since 2018 also individual rare-earth ions. The latter are of particular interest as they constitute the only solid-state defect with long optical coherence time, a requirement for the creation of efficiently multiplexed QM for light[66].

To create true single photons, the conceptually simplest approach is to excite a single atom, ion or optical centre, and to wait for subsequent spontaneous emission. However, due to their long excited state lifetimes, often ms, along with the fact that spontaneous emission is undirected, this approach is very inefficient for rare-earth ions. Yet, by coupling the ion to the mode of a cavity with small mode volume V and large quality factor Q, resulting in the modification of the ion's electromagnetic environment, it is possible to increase the emission rate and furthermore to direct the emission into a mode that is defined by the cavity. This is called the **Purcell effect**[97]. The enhancement of the emission rate is given by the ratio of the cavity density of states to that of free-space, the Purcell factor F_P, and can be expressed by

$$F_P = \frac{3}{4\pi^2}\beta\left(\frac{\lambda}{n}\right)^3 \frac{Q}{V}\frac{|E(r)|^2}{|E_{max}|^2}. \quad (1)$$

Here, β is the branching ratio of the desired transition, n is the refractive index of the crystal, and $E(r)$ and E_{max} denote the field at the position of the ion and the maximum electric field, respectively. Note the assumed optimized polarization. The reduction of the lifetime T_1 furthermore yields the potential of achieving radiation-limited emission with $T_2 = 2T_1$ (with coherence time T_2).

While difficult with traditional cavities, Purcell-enhanced emission and the observation of single photons from individual rare-earth ions has become possible due to the emergence of micro- and nano-scale cavities with mode volumes in the order of λ^3 or smaller. Starting with standard semiconductor platforms such as Si[98], fabrication methods for photonic crystal nanocavities[99] have lately been extended, e.g. to diamond[100][101], yttrium orthovanadate[102] and $LiNbO_3$[103][104][105][106]. In parallel, open microcavities with sufficiently small mode volumes have been developed[56][107], which would allow the use of any rare-earth material.

To achieve Purcell-enhanced emission based on photonic crystal cavities, two approaches are being pursued. First, it is possible to create the nanocavity directly out of the rare-earth crystal, either by means of focused ion beam milling[32] or through reactive ion etching[35]. In this case, the coupling between the light and the rare-earth ion happens inside the cavity where the electric field is highest and E(r) approaches E_max. Alternatively, one can also fabricate a cavity out of a material without rare-earth doping, and then transfer the cavity onto the rare-earth-doped crystal[31]. In this 'heterogeneous' approach, the coupling with a single ion is mediated via the evanescent field, which is smaller than in the 'homogeneous' case where the ion is located within the cavity. Note that the addressable rare-earth-ion transitions are limited in both cases to the transparency window of the (external) cavity. In the case of silicon, currently the most widely used material, this excludes wavelengths below 1.1 μm and hence the transitions in Eu (λ ≈ 580 nm, depending on the host crystal), Pr (λ ≈ 606 nm), Tm (λ ≈ 794 nm) and Yb (λ ≈ 980 nm) that are currently being investigated for optical QM[66][108][109][110].

determine compatibility with QM and transmission over optical fibre or free-space links. Note that it may be necessary to change the wavelength of the emitted photons as it will in most cases only be compatible with either the absorption line of a QM or the transparency window of the transmission medium, but not with both. An exception are erbium-based sources, which allow emitting photons at telecom wavelength of 1532 nm that are obviously also spectrally compatible with erbium-based QMs (see section 5.3 for more info about Er-based memories). Otherwise, the required frequency conversion can be implemented by means of a non-linear interaction between the photon to be converted and a strong laser pulse[111][112][113]. Additional figures of merit include a high probability of creating true single photons, the latter being generally assessed in terms of the autocorrelation coefficient $g^{(2)}(0)$, where, ideally, $g^{(2)}(0) = 0$.

Currently, the largest challenge is to achieve indistinguishability, which is at the heart of multi-photon interference[53]. In turn, indistinguishability enables the creation of heralded entangled photons using four single photons[18], the entangling operation in the link nodes (see figures 2 and 3), and quantum teleportation between repeater nodes[29][81], to name just a few applications. Of particular concern is spectral purity, i.e. the realization of a Fourier-limited and stable spectrum, free of spectral diffusion.

And finally, being an important criterion for any quantum technology to become a real-world application, single photon sources must become scalable and easy to use.

4.4. Single photon sources, state-of-the-art

Starting with the first two demonstrations in 2018[31][32] single-photon detection based on Purcell-enhanced light–matter interaction has now been reported by several groups[29][33][34][35][36][37][38][39][40][114][115] see [41] for an alternative approach). However, only two groups could so far demonstrate the indistinguishability of subsequently emitted photons from the same rare-earth ion[29][39]. Furthermore, the possibility of quantum interference with photons from two different sources, which underpins the functioning of quantum networks and especially of quantum repeaters, has only been reported once[29]. The problem is spectral diffusion, which leads to broadening of the photons' spectra beyond the limit imposed by the radiative emission rate γ. This results in distinguishability and prevents two-photon interference.

Spectral diffusion is a common problem for all solid-state emitters and has been suggested to be particularly pronounced for rare-earth ions close to surfaces[39], as is the case in nanophotonic structures. To limit spectral diffusion due to time-varying electric fields, the above demonstrations of indistinguishability and interference[29][39] were therefore based on crystals in which the rare-earth ions occupy sites with non-polar symmetry. Another, or an additional, strategy is to use open micro-cavities as in, where relatively thick crystals allows interacting with rare-earth ions that are far away from surfaces[34]. However, some authors reported that no such ‘nanostructure-enhanced’ spectral diffusion has been observed in crystals with polar symmetry where the effect should be more pronounced[116]. In addition, it has also been proposed that the use of ions within the tail, not the centre, of the inhomogeneously broadened absorption line, for which strain may impact the site symmetry, could lead to additional spectral sensitivity[117]. This leaves the question of how to minimize spectral diffusion in order to create indistinguishable single photons currently open.

5. Network components: ensemble-based QM for light

The quantum repeater in figure 2 requires one to delay, or store, photons until the results of measurements of other photons become available. The minimum required delay is given by the round-trip communication time set by the speed of light, but can be significantly longer due to photon transmission loss and other inefficiencies[25][118]. The storage of photons allows conditional operations, also referred-to as feed-forward control. To optimize the entanglement distribution rate, it should be possible to continuously add photons to the memory, i.e. the memories should be multimode[52][118]. Atomic ensembles with a large number of atoms such as rare-earth ion-doped crystals are natural candidates for the required storage as they allow one to reversibly map a large number of temporally, spectrally or spatially multiplexed photons onto different collective atomic modes with negligible overlap[119][120][121].

5.1. Photon echo QM with rare-earth-ion ensembles

An important class of QM protocols that lends itself ideally to materials with inhomogeneously broadened optical absorption lines such as rare-earth doped crystals stems from the photon-echo protocol[122]. ‘Photon-echo quantum memory’ relies on the transfer of the optical quantum state onto a collective atomic excitation. Assuming the absorption of a photon in an ensemble of two-level atoms at time t_0, the atomic state becomes[23]

where N is the total number of atoms, and g_j and e_j denote the ground and excited state, respectively, of atom j. The wave number of the optical field is given by k, z_j is the position of atom j, and c_j characterizes the frequency and position-dependent coupling of atom j to the field. Since dealing with an inhomogeneous ensemble, each atom has a different detuning δ_j of the atomic transition with respect to the optical carrier frequency, which causes inhomogeneous dephasing of the state in equation (2) after the absorption of the photon. Often seen as a nuisance, this can in fact be used as a resource for multiplexing. For instance, in the time domain, l photons absorbed at different times t_0 will each create collective states of the same form as in equation (2), but they are distinguishable by their different start times t_0. Similarly, photons in different spatial modes k will generate distinguishable collective states. To map these atomic excitations back onto optical modes, i.e. to trigger the re-emission of the stored photons, the inhomogeneous dephasing must be undone. All photon-echo type QM protocols employ a specific method to achieve the required rephasing. In the following focus on the **atomic frequency comb** (AFC) scheme, the currently most widely implemented protocol, but will also briefly mention alternative protocols.

The AFC protocol is based on an inhomogeneously broadened absorption line tailored into a periodic series of narrow absorption peaks[120] with detuning δ_j = m_j Δ, where m_j is an integer and Δ is the comb periodicity. Such an AFC can be created by persistent spectral hole burning (SHB) techniques, where recently developed techniques have allowed the creation of broadband and high resolution AFC structures[123][124]. An incoming photon is absorbed by the comb, with the comb bandwidth Γ matching the photon bandwidth. Thanks to the comb periodicity, it follows directly from equation (2) that the collective state rephases at a time t = 1/Δ, causing photon re-emission (output) in the form of the AFC echo. This 2-level AFC echo acts like a delay line with pre-determined storage time, the on-demand read out based on the 3-level AFC will be discussed below.

A key feature of the AFC scheme is its high temporal multimode capacity. The number of temporal modes N_t that can be efficiently stored only depends on the number of teeth in the comb N_{teeth}, the capacity being $N_t = N_{\text{teeth}}/2.5$[121]. To maximize the temporal mode capacity, one should thus look for materials with narrow homogeneous linewidth, i.e. long optical coherence time, and large absorption bandwidth.

The efficiency of an ensemble-based QM depends on the collective light–matter coupling, i.e. it depends on the optical depth of the ensemble[120][125][126]. Here is need to distinguish forward and backward recall, the efficiency for forward recall being $\eta_{\text{AFC}} = \bar{d}^2 \exp(-\bar{d})\eta_d$[120], where $\bar{d}$ is the effective optical depth averaged over the AFC and η_d a dephasing factor determined by the shape of a single tooth[120], whose width is limited by the inverse coherence, the homogeneous linewidth. For backward recall, which can be achieved by phase matching and auxiliary control fields[48], the efficiency is given by $\eta_{\text{AFC}} = (1 - \exp(-\bar{d}))\bar{d}\eta_d$. For forward recall, the efficiency is limited to 54% due to the re-absorption factor $\exp(-\bar{d})$[125], while for backward recall it can approach 100% for high optical depth and high comb finesse[120][125]. An alternative method to reach high efficiency is to put the memory in a single-sided optical cavity whose input mirror is impedance matched to the memory absorption[127]. In this way, unit efficiency can be approached without resorting to the phase matching operation of backward recall, even for a moderate cavity finesse. For a perfectly impedance-matched, loss-less cavity, the efficiency is only limited by the intrinsic AFC dephasing factor $\eta_{\text{AFC}} = \eta_d$[128], which can approach unity for high enough AFC finesse.

An alternative rephasing method, the so-called gradient echo memory (GEM) protocol[129] (which is closely related to the **controlled reversible inhomogeneous broadening** (CRIB) protocol[130][131]), allows forward recall that is not limited by re-absorption. However, GEM/CRIB memories have less temporal multimode capacity with respect to AFC memories[119].

The collective state in equation (2) can also be rephased using optical π pulses. The method called **revival of silenced echo** (ROSE)[132] is a variant of the two-pulse photon echo and avoids in principle population inversion and hence spontaneous emission noise during the echo emission. However, in practice, imperfect π pulses cause such noise[133], and the potential of ROSE for quantum state storage remains an open question. To overcome this problem, the **noiseless photon echo** (NLPE) protocol was recently proposed[134], where a 4-level system is employed instead of the 2-level system in ROSE. The advantage of NLPE with respect to AFC is that no initial memory preparation step (SHB) is required, which removes complexity and leads to higher efficiencies thanks to a higher effective optical depth[134]. However, the 4-level scheme adds dephasing with respect to the AFC scheme due to uncorrelated inhomogeneous broadening of the employed transitions, which reduces the optical storage time and hence the temporal multimode capacity with respect to an AFC memory in the same material[134].

For a QM that exploits a single optical transition, the storage time is limited by the optical coherence time T_2. In the case of rare-earth crystals, T_2 can reach ms[65][66][135], a unique feature among solid-state centres. Even longer storage times can be achieved when mapping the optical coherence in a reversible manner onto hyperfine states using optical control π-pulses, a technique that is generally referred-to as 3-level (or spin-wave) AFC protocol[120][136]. Moreover, for AFC memories this also allows readout-on-demand, which is not possible in case of the conventional 2-level AFC scheme, although some degree of control of the read-out time can be achieved

pulses[142]. In the simplest version, the spin-wave memory storage time is limited by inhomogeneous dephasing of the hyperfine transition, typically on the order of tens of µs[136][141]. The storage time can be extended to the spin coherence time by applying two π pulses on the hyperfine transition[142]. By dynamically decoupling the hyperfine transition from the perturbing environment using many π pulses the storage time can be extended further[143], possibly up to the ultimate limit of 2T.

To finish this section, let us also mention 'photon emission'-based approaches for multimode light–matter entanglement generation, i.e. the RASE[144] and AFC-DLCZ protocols[145]. Here, the atomic system acts as both a source and memory for pairs of photons. These schemes have large temporal multimode capacity and include the possibility for extended spin-wave storage. However, the sources are probabilistic, featuring the same issues as sources based on SPDC (see section 4.1). Finally, note that storage via electromagnetically induced transparency (EIT) has been explored for long-duration single photon storage[146]. Yet, due to their limited temporal multimode capacity[119], EIT-based memories are less attractive for quantum networks.

5.2. Figures of merit

A large number of figures of merit can be used to characterize the suitability of a QM for a quantum repeater link. Below discussing the most frequently used ones, and provide some information relevant to their realization using the AFC QM protocol in rare-earth-ion doped crystals.

Storage efficiency.

The memory efficiency is a key metric for quantum repeaters, as the final rate will scale with the memory efficiency to the power of the number of memories employed in the repeater link (the exact scaling depends on the specific repeater scheme). Therefore, many repeater rate simulations assume memory efficiencies of 90%[25], although some works have considered lower efficiencies[147]. Note that the storage efficiency η_M decreases as a function of storage time τ due to atomic dephasing with some characteristic memory lifetime T_m. Assuming a 2-level AFC with Lorentzian-shaped teeth of T_2-limited width, one can show that $\eta_M = \exp(-\tau/T_M)$ with $T_M = T_2/4$[123].

Storage time.

The required storage time depends on the repeater protocol and imperfections in the implementation. In the ideal case with large multiplexing, it is given by the time it takes a photon to travel from a repeater node to a link node, and classical information to travel back [52]. Assuming an elementary link length of 100 km, a reasonable assumption for a fibre-based quantum network in Europe where cities, and hence access points to the network, are close, this amounts to 500 µs. However, transmission loss and device inefficiencies paired with insufficient multiplexing reduce the probability with which entanglement is heralded across each elementary link within the round-trip time, resulting in the need for longer storage times[147]. For 2-level AFC storage, the storage time is limited by the optical coherence time, see the discussion of the storage efficiency above, while for 3-level AFC it is limited by the spin coherence time[142].

Post-selected fidelity.

The fidelity is defined as $F = \mathrm{tr}(\langle\psi|\rho|\psi\rangle)$, where $|\psi\rangle$ denotes the input qubit state and ρ the density matrix of the output qubit, conditioned (i.e. post-selected) on the detection of an emitted photonic qubit. The 2-level AFC scheme can be made virtually noiseless, in particular, atomic decoherence does not affect the state of a re-emitted photon[137][148][149], resulting in very high post-selected fidelities, e.g. 99.9% in[150]. In case of the 3-level protocols (3-level AFC, RASE and NLPE), the storage process is generally not noise free but the fidelity is affected by the quality of the π pulses[141][142]. Storage fidelities in the range of 75%–85% have been reported[108][151] for AFC spin-wave memories and above 90% for NLPE memories[134][152]

Feed-forward mode-mapping.

This figure of merit addresses the necessity to modify the mode of a photon that is entangled with a second photon on the other end of an elementary link after their entanglement has been heralded by the Bell state measurement at the intermediate link node. The goal of the mode-mapping operation is to make the two photons that belong to entangled pairs in neighbouring links indistinguishable so that the subsequent Bell-state measurement, which extends entanglement across these two (or more) links, can be performed. In many repeater schemes, temporal multiplexing is assumed and entanglement across neighbouring elementary links is heralded at different times[25][118]. In this case, it is necessary to dynamically tune the moment of arrival of the re-emitted photons at the Bell-state measurement. This can be achieved using on-demand readout as in the 3-level AFC protocol, or by means of rapidly switchable optical

memories (no temporal mode mapping), spectral multiplexing and frequency shifters plus filters.

The wavelength of operation.

The wavelengths of rare earth ions that are currently of most interest for QMs are λ ≈ 580 nm (Eu), 606 nm (Pr), 794 nm (Tm), 980 nm (Yb) and 1530 nm (Er). With the exception of erbium, they differ from the wavelength at which fibre transmission is maximized. When using a photon pair source based on SPDC or four-wave mixing, this difference can be bridged by designing the source to create non-degenerate photon pairs with one photon optimized for fibre transmission and one for storage[154][155]. However, as described in section 4.1, these sources are probabilistic, which impacts the rate with which entanglement can be established across a long and lossy quantum channel. For repeater schemes based on single photon emitters[156] or on frequency-degenerate entangled photons, quantum frequency conversion allows changing the wavelength of the photon travelling to the link node, to the memory, or both, as described in section 4.3.

The storage bandwidth per spectral channel.

The storage bandwidth sets the minimum duration of a photon that can be stored. It therefore puts a constraint on the required bandwidth of external photon sources interfaced with the memory. In the case of the AFC protocol, the bandwidth is limited by the energy splitting of the hyperfine states employed for the SHB, although in some specific cases it can be made larger[157]. For non-Kramers ions such as Pr and Eu, bandwidths are typically limited by nuclear hyperfine splitting to less than 10 MHz[121], but bandwidths in excess of 1 GHz can be achieved in Tm-doped crystals[89] due to much larger Zeeman splitting. For Kramers ions such as Yb, the bandwidth can be larger, e.g. 100 MHz in Yb:Y_2SiO_5[124]. Finally, a note that by matching the AFC tooth spacing with the level spacing, even larger bandwidths can be obtained, e.g. 5 GHz in Er:$LiNbO_3$[155] and 10 GHz in an erbium-doped fibre[158], however, at the expense of a limited storage efficiency.

The multiplexing capacity.

For efficient entanglement distribution, the total multiplexing capacity should be large[25][52][118]. Photons can be stored in a combination of temporal (N_t), frequency (N_f) and spatial (N_s) modes, resulting in a total capacity $N_{\text{tot}} = N_t N_f N_s$. For instance, assuming $N_t = 1000$ temporal modes, e.g. for a photon duration of 500 ns and optical storage time of 500 μs, $N_f = 100$ frequency modes and $N_s = 10$ spatial modes, find a total number of modes of $N_{\text{tot}} = 1000000$. Reproducibility and ease of use also play important roles for the creation of large scale networks and for future commercial exploitation. This includes properties like temperature of operation, footprint, and the possibility for integration with other network components. Their solid-state character makes rare earth systems in general very attractive, and the possibility for on-chip integration[155][159][160] yields additional possibilities.

5.3. QM experiments state-of-the-art

The following section focuses on experimental demonstrations of optical QM using ensembles of rare-earth-ions. It focuses mostly on implementations of the AFC protocol with single or entangled photons, but it also includes notable demonstrations with classical laser pulses and based on other approaches.

Starting with the first experimental demonstration of the 2-level AFC scheme at the single photon level[149], progress has been very rapid. Key demonstrations of 2-level AFC memories include storage of energy-time[154][159] or time-bin entangled photons[155][162], storage of single-photon polarization qubits[150][163][164][165], storage of hyper entanglement[166], teleportation of a qubit into a memory[167][168][169], non-local gates with QM[170], light–matter entanglement distribution over a metropolitan fibre[171] and entanglement of two AFC QMs[172][173][174][175]. Temporal multimode storage range from 62–100 stored modes[121][174][176][177] to more than 1000 modes[124][158][178]. Multimode storage has also been demonstrated using spatial[179] and spectral[52][180] degrees of freedom, as well as a combination of all three degrees-of-freedom[181]. Furthermore, storage efficiencies around 40% have been reported[121][182] with the crystal in a free-space configuration, and cavity-enhanced storage efficiencies of 53%–62% have been achieved for attenuated laser pulses[109][128][183] and of 27% for heralded single-photon states[184]. The highest reported efficiency of 69% has been demonstrated with GEM[185].

AFC spin-wave storage has first been reported with weak coherent states at the single photon level[141][142] and recently also with entangled photons[151]. A cavity-enhanced AFC spin-wave experiment has reached 12% efficiency[128], and dynamical decoupling has allowed storage of time-bin qubits with a fidelity of 85% for up to 20 ms at the single-photon level[108] and storage of classical laser

quantum correlations and entanglement.

Erbium-based Quantum Memories

Erbium-based QMs are of particular interest as they operate directly in the telecom C-band at 1532 nm wavelength. QM protocols have been demonstrated in several Er-doped systems, e.g. storage of attenuated laser pulses in $Er^{3+}:Y_2SiO_5$ based on CRIB[167] and in [167]$Er^{3+}:Y_2SiO_5$ based on AFC 2-level memories[160][193]. Furthermore, entangled photons have been stored in AFC 2-level memories in an erbium-doped fibre[158][162][173], in $Er^{3+}:LiNbO_3$ [194][195] and in $^{167}Er^{3+}:Y_2SiO_5$[196]. Non-classical multimode correlations have been demonstrated using RASE in [167]$Er^{3+}:Y_2SiO_5$[188], with a recall efficiency of 17% (up to 80% recall efficiency in a classical regime). However, Er-doped fibre QMs are hampered by short optical coherence times[197], due to its amorphous property. In Er-doped crystals, the spectral holeburning efficiency at low magnetic fields at low magnetic fields has been limited by short spin-lattice relaxation between the electronic Zeeman states[198][199]. However, recent experiments have shown 0.55 s spectral hole lifetime in $Er^{3+}:LiNbO_3$ at 13 mK and 1.3 T[195]. In addition, it was shown that electronic spin relaxation in [167]$Er^{3+}:Y_2SiO_5$ can be quenched at sufficiently high magnetic field, resulting in around 70 s spectral hole lifetime above 3 T at 1.4 K[62] and allowing one to prepare efficient QMs[193]. Storage time as a function of the efficiency for several of the above-mentioned QM realizations. While overly simplifying the requirements of a QM for a quantum repeater and focusing only on AFC-based memories, it provides nevertheless some useful insights. The data is extracted from a total of 5 papers, reporting recent results from 2-level AFC-type storage with[109] and without cavity[66][108][110], and 3-level AFC-based storage with[108][110][161] and without[151] spin control pulses. a note that included demonstrations in which single photons, attenuated laser pulses as well as strong laser pulses were stored. While it is true that storage of strong laser pulses is much easier than storage of true quantum states of light, the protocol steps remain the same. For the purpose of this paper, therefore ignore this difference.

As a benchmark for comparison, use the case of a (readily available) telecom optical fibre with absorption coefficient of 0.2 dB km^{-1}. The transmission through such a simple delay line, equivalent to the storage efficiency, is given by

$$t_{\text{fibre}} = 10^{-0.02\ell} \quad (3)$$

where ℓ is the fibre length in km. Clearly, for an atomic QM to be useful, its efficiency has to be higher than the fibre transmission for the same delay. Several observations are noteworthy.

For storage times below 400 µs, no memory implementation currently beats the simple fibre delay line in terms of storage efficiency. However, the gap has narrowed significantly over the past few years, e.g. to less than a factor of two in the case of cavity-enhanced memory with small storage time[109]. For storage times beyond 400 µs, the atomic memories perform better than the fibre delay line. Still, the storage efficiencies need to be improved to make these memories useful for quantum repeaters.

The efficiencies in the implementations of the 2-level AFC protocol in materials with optical coherence times above 1 ms[66][108][167] decrease faster than what one would expect from this coherence time. This currently limits storage times to around 100 µs even though memory lifetimes T_M around 300 µs should in principle be achievable. The reasons for the reduced lifetime are spectral diffusion, cryostat vibrations, and laser line jitter. These issues also limit the time during which quantum information can be stored in optical coherence in the 3-level AFC protocol[121], which in turn limits the multimode capacity.

Assuming that the first quantum repeater generation will employ probabilistic SPDC-based entangled photon pairs with small photon pair generation probability, the required memory storage times will be long compared to the round-trip time from a repeater node to a link node and back[118]. This is required to ensure that heralded entanglement across adjacent elementary links will eventually be created. Such storage times, around 100 ms in[147], will require using the 3-level AFC protocol with spin wave control such as in[108], as well as cavity-enhanced light–matter interaction as in[109].

Once efficient and sufficiently multimode photon sources are available, shorter storage times will suffice. Ideally, the storage time equals the round-trip time mentioned above.

- For fibre-based quantum communication in densely-populated areas, it makes sense to space link nodes at intercity distances, e.g. between a few tens of kilometres to hundred kilometres. This yields storage times of a few hundred µs, which is possible using the 3-level AFC protocol but is also getting into reach of 2-level AFC implementations.
- For quantum communication through long-haul fibres or operating over satellite-based communication links, the distance between nodes and hence the round-trip times will be much longer, e.g. a few thousand km and around 10 ms in the case of a satellite, respectively. These storage times require the use of the 3-level AFC protocol together with spin-wave control. First demonstrations[108][161] show that this may be feasible in near future.

feasible, but storage efficiencies still require significant improvements.

In summary, find that QMs based on ensembles of rare-earth ions are likely to become rapidly useful for quantum repeaters over optical fibres and free-space links, and hence also for extended quantum networks based on a combination of those.

6. Network components: repeater nodes with quantum processing capability

Previously described repeater nodes based on ensemble memories. In this section, is described repeater nodes composed of individual ions that encode long-lived qubits and allow quantum information processing.

The potential of rare-earth ions for quantum gates and quantum computing was first pointed out in 2002[200] (see[30] for a recent review). Qubits can be encoded into nuclear spin states of individual ions, whose coherence times in strong magnetic fields can reach 6 h[27]. Furthermore, ion spacing of as little as a few nanometres, either naturally or through deterministic ion implantation[201], enables efficient qubit–qubit interactions. The proximity, however, creates a problem with the need for individual addressing. This can be circumvented in an elegant manner by using optical control pulses, which results in spectral selectivity due to the inhomogeneous broadening of the optical transitions[200]. Infidelities for single and controlled two-qubit gates have been predicted to be of around 10^{-4} and 10^{-3}, respectively[202][203], allowing one in principle to create high-fidelity spin-photon entanglement and in turn entanglement between distant spins using the Barrett-Kok scheme[20]. In addition, using controlled interactions between neighbouring ions, it may be possible to reach the noisy intermediate scale quantum domain[204]. Initial experimental work focused on demonstrations using large ensembles[205], but this does not scale to multiple qubits[206]. Instead, scalable quantum information processing requires the individual ion regime, which has historically been difficult to reach with rare-earth systems due to their long excited-state lifetimes. However, in recent years there has been significant progress, and many research groups are now routinely investigating single rare-earth ions. Towards this end, it is important to collect a strong fluorescence signal, which can be achieved using cavity-enhanced transitions and the Purcell effect discussed in section 4.2.

The recent breakthroughs in detecting single ions allow for a different type of repeater nodes than what has been discussed above, more precisely repeater nodes in which quantum information is stored in qubits capable of information processing. refer to these nodes also as quantum processor nodes. In view of building a quantum repeater, the main advantage of using quantum processor nodes is that they open up the possibility for deterministic, as opposed to probabilistic[47], entanglement swapping operations between neighbouring elementary links, however, at the expense of less multiplexing across each individual elementary link.

Quantum repeaters based on individual ions employ three main steps, which are illustrated in figure 3, briefly described below, and discussed further in sections 6.1–6.3.

- **Qubit–photon entanglement:** Individual qubits in repeater nodes are entangled with single photons.
- **Photonic entanglement swapping:** Through photon interactions and measurements, the qubit–photon entanglements are swapped into entanglement between qubits in adjacent nodes.
- **Deterministic qubit–qubit entanglement swapping:** Joint operations and measurements on two neighbouring qubits in the same quantum repeater node, each entangled with a qubit in another node, enable deterministic entanglement swapping across adjacent elementary links.

6.1. Qubit–photon entanglement

This section discusses two main ways in which qubits can be entangled with single photons. In the first method, qubits are put into superposition states and used as emitters of single photons so that the state of the ion is entangled with the emitted photon. This protocol may rely on an individual ion acting as both the photon emitter and the long-lived qubit, as in the case of trapped ions[50] and diamond colour centres[7]. Ideally, the emitter features a Purcell-enhanced optical transition that should additionally be at telecom wavelength, although it is possible to frequency convert photons at the cost of added complexity (see section 4.3). However, Purcell enhancement reduces the excited state lifetime, while the controlled two-qubit gate assumed in[56] and described in section 6.3 benefits from long lifetimes and narrow optical transitions. Thus, it can be beneficial to use two different ion species: one for communication and one for storage[56][207][208]. Attractive candidates for communication ions are Er due to its telecom transition and Nd due to its large oscillator strength in many hosts[209], whereas Eu is a strong candidate for encoding qubits due to its long spin lifetimes[67] and spin coherence times[27]. Other potentially interesting ions are Yb due to its reduced sensitivity to magnetic fields, Yb features a zero first-order Zeeman transition at zero magnetic field[63], and Tm, which, in certain crystals, features ZPLs that connect the ground state with different excited states[210], one of which could be Purcell enhanced and one of which could be kept spectrally narrow.

that these demonstrations, which were done using diamond colour centres or trapped atoms, can be generalized to rare-earth ions.

6.2. Photonic entanglement swapping

Consider the case when qubit-photon entanglement is created using the first method described in the previous section, i.e. where qubits are used as emitters of single photons. Qubits in adjacent repeater nodes can then be entangled by sending the photons to a link node where they are subjected to a probabilistic linear-optics Bell-state measurement, as in the ensemble-based scheme discussed above. This swaps the entanglement from two qubit-photon pairs in a heralded fashion to the qubit-qubit pair. Without additional resources this process is probabilistic, however, please recall that this measurement, but not the transmission of photons across the elementary link, can in principle be achieved deterministically by adding auxiliary entangled photons[54][55].

When both communication and storage ions are used, the end goal is to entangle storage ions, and will now describe two approaches to achieve this. Either one first entangles two communication ions in adjacent repeater nodes using, for instance, the Barrett–Kok scheme[7][20], and then one swaps the entanglement to the storage ions[207]; or one starts by locally entangling the storage ion with the photon emitted from the communication ion and then attempts entanglement swapping by measuring two photons in a link node[56]. In the former case, the communication ions must remain idle with good coherence properties during the time it takes the photons to travel to the link node and the classical heralding information to return. Provided that entanglement has been established across the elementary link, it is swapped to the storage ions, and one can attempt to entangle the communication ion with another processor node. The benefit of this approach is that it only requires one communication ion and one storage ion per node. Conversely, the latter method has the advantage of freeing up the communication ion immediately after it has emitted a photon, thus relaxing the coherence requirements of the communication ion. Furthermore, if additional storage ions are available, the protocol allows for time multiplexing by reusing the communication ion to emit new photons entangled with other storage ions.

Alternatively, if the second method described in the previous section is used, qubit-qubit entanglement can be achieved via a deterministic entangling operation implemented by means of state-dependent reflections of a time-bin photonic qubit from a cavity coupled to an individual ion[21].

6.3. Deterministic qubit–qubit entanglement swapping

Deterministic entanglement swapping between qubits in repeater nodes can be achieved as long as two-qubit gates and qubit measurements can be performed on the two qubits involved in the entanglement swapping in a node[213].

Provided the two qubits are sufficiently close and that their states feature permanent electric dipole moments, two-qubit gates can be implemented using the electric dipole-blockade. For example, a CNOT gate can be realized by first exciting the control qubit from $|0\rangle \rightarrow |e\rangle$, then attempting a NOT operation on the target, before finally de-exciting the control from $|e\rangle \rightarrow |0\rangle$. Due to the blockade effect, the NOT operation on the target is only possible if the control is in state $|1\rangle$. The key to this gate is that the transition of the target qubit from $|0\rangle$ to $|e\rangle$ is spectrally sufficiently narrow to ensure that a small Stark shift $\Delta\nu$ detunes it out of resonance with the lasers used for the NOT operation. Alternatively, magnetic dipole–dipole interactions can be used, either between weakly interacting spins of two adjacent rare-earth ions or between the electron spin qubit and nearby nuclear spins of the host. This basic interaction has recently been demonstrated in rare-earth systems[214][215].

The capability of performing two-qubit gates additionally allows for entanglement purification protocols[216][217][218][219], and if there are sufficiently many storage qubits and the operations are sufficiently good, one can even consider performing error correction within nodes[220][221] to improve the fidelity and efficiency of the quantum network. Initial theoretical work that focuses on the specific properties of rare-earth ions has already been reported[222].

6.4. Figures of merit

This section focuses on the figures of merits of quantum processor nodes. Some of these merits are similar to the ones already discussed for QMs, including the wavelength of operation and the storage time, whereas others are different, and those are briefly discussed here. Importantly, in contrast to the case of QMs, the storage efficiency is no longer relevant, and atomic decoherence impacts the fidelity instead.

- **Fidelity of the entangled operation between two nodes.** It is possible to use SPDC sources for qubit-based protocols, for example using the photon reflection techniques[21] with cavities. In this case, there is a trade-off between the entanglement fidelity and the entanglement rate, as discussed in section 4.1. For repeaters based on qubits that emit single photons, this trade-off is removed, and the entanglement fidelity is instead limited by the quality of the single photon emission, single photon purity and indistinguishability between photons. together with the fidelity of the qubit gate operations.

directly entangled with storage ions.

- **Photon bandwidth.** In protocols that use only a single ion type as both emitter and qubit, the photon bandwidth may be limited by the energy level spacing between the qubit levels, in similarity with some of the ensemble-based protocols. Protocols that directly entangle emitted photons with storage ions avoid this limitation. However, a similar restriction arises if the communication ion interacts with the qubit ion using the dipole blockade mechanism, as the dipole frequency shifts must be larger than the bandwidth of the optically excited state of the communication ion.

6.5. Quantum processing nodes, state-of-the-art

Despite the first demonstration of cavity-enabled single ion detection being only a few years old, there have already been significant advances. Several groups have achieved single-shot readout of individual spin qubits, for example in Er-doped silicon[223], Er-doped Y_2SiO_5[224], Yb-doped YVO_4[117], and four Er ions doped in Y_2SiO_5 have also been simultaneously initialized and read out in[33]. Furthermore, coherent spin manipulation of individual ions has also been demonstrated[33][117].

In[215], a Yb ion was coupled to an ensemble consisting of four equidistantly spaced V host ions, and via a spin-exchange interaction, the authors could generate collective spin excitations of the ensemble and use it as a QM. Furthermore, they were able to prepare and measure maximally entangled Yb–V Bell states.

Controlled interactions have also been shown in Er-doped Y_2SiO_5[214], where a single Er ion interacted with a I = 1/2 nuclear spin in the host crystal, identified as a fortuitously located proton (^1H). Through the use of dynamical-decoupling sequences applied to the electron spin, the nuclear spin could be controlled and both single- and two-qubit gates performed.

Another crucial aspect required for repeater nodes based on quantum processors is the interaction between individual ions and single photons. As discussed previously, this can be achieved through state-dependent reflections of photons from a cavity coupled to an individual ion[21], but a demonstration of such a protocol using rare-earth ions is still missing. However, entanglement between an individual Er and an emitted photonic time-bin qubit has recently been reported[28]. Furthermore, two Yb ions located in two separate nanophotonic cavities have been entangled via a joint measurement of two emitted photons[29]. In this latter work, the authors also demonstrated probabilistic quantum state teleportation between the two Yb qubits, and generated a tripartite W-state between three Yb spin qubits (two located in one nanophotonic cavity and one located in a second cavity).

7. Elementary quantum repeater links

In this section, are briefly discuss experiments with rare-earth systems that aim at the demonstration of an elementary quantum repeater link, i.e. experiments where at least two QMs were entangled. Note that demonstrations of entanglement between photons and a single QM are already discussed in section 5.3.

Entanglement between two separate rare-earth systems was reported for the first time in 2012[172]. A single-photon entangled state was generated by splitting a heralded photon, generated by means of SPDC, between two spatial modes. Each mode was stored in a separate QM using the 2-level AFC protocol, resulting in a single excitation delocalized, or entangled, between two Nd^{3+}:Y_2SiO_5 crystals separated by 1.3 cm. The storage time in this demonstration was 33 ns. While this creation of memory-memory entanglement was heralded by a photon detection, the scheme is not scalable to large distances between the crystals without losing the efficiency of the heralding process.

In 2020, another group reported the storage of both entangled photons from an SPDC-based source, again employing the 2-level AFC protocol[173]. In this demonstration the two photons featured different wavelengths, requiring the use of two different rare-earth memories: a Tm-doped crystal for the 794 nm photons and an Er-doped crystal for the 1535 nm photons. Storage times in this proof-of-principle demonstration, 32 ns and 6 ns, respectively, were again short. In this case, the storage process was not heralded, as opposed to the requirement for an elementary repeater link described in section 2.2.

Several shortcomings of these two demonstrations were overcome in 2021, when two groups demonstrated the heralded creation of entanglement between two crystals, in line with the repeater architecture depicted in figure 2[174][175]. In both demonstrations, each of two SPDC sources emitted one photon per pair into a 2-level AFC QM and the second photon over optical fibre to a central linear optics Bell-state measurement. Subsequent photon detection then heralded entanglement between the two memories.

In[175], two Nd^{3+}:VO_4 QMs were employed to store photons at 880 nm during 56 ns, and the Bell-state measurement was based on the detection of 2 photons. While the demonstration did herald entanglement between the stored and subsequently recalled photons, the combination of such a two-photon Bell-state measurement with photon pairs generated by means of SPDC implies that this elementary

Single-photon schemes, on the other hand, complicate the entanglement verification and require interferometric stability of the fibre link[225]. The demonstration relied on two $Pr^{3+}:Y_2SiO_5$ memories that stored photons at 606 nm wavelength up to 25 µs, including in multimode fashion. Note that the wavelength of the second member of each photon pair was 1436 nm, which, in principle, would allow long-distance entanglement.

Even more recently, the first demonstration of an elementary repeater link based on individual rare-earth ions was reported[29]. This work is particularly noteworthy as it showed for the first time that spectral diffusion can be overcome through the combination of a crystal with rare-earth sites that feature reduced sensitivity to electric field noise (see discussion in section 4.4) and active spectral control. Using two Yb ions in separate YVO_4 crystals and a Bell-state measurement based on the detection of a single photon, the researchers did not only demonstrate heralded entanglement that lasted for almost 10 ms in a scalable fashion, but also quantum teleportation as well as the creation of a tripartite entangled state, which required adding a third ion.

To finish this brief review of developments related to the creation of elementary quantum repeater links, let us also mention the demonstration of interference of weak laser pulses recalled from separate $Tm:LiNbO_3$-based QMs[226]. In contrast to the above-described experiment, this demonstration targeted the connection between neighbouring elementary repeater links.

8. Conclusion and outlook

In this review is detailed the progress towards quantum repeater networks made so far using the rare-earth-ion based platform. Here briefly conclude by providing some suggestions for future work.

- **Single emitter:** Starting with the first demonstrations of Purcell-enhanced emission in 2018, the development of single rare-earth ions as sources of individual photons has been very rapid, and emitters at telecom wavelength around 1532 nm (Er), at around 980 nm (Yb), and at around 880 nm (Nd) have been demonstrated. However, some of the best rare-earth-ion based QMs employ Pr, Eu and Tm, and more work is required to develop photon emitters using these ions. This will allow overcoming the limitations of SPDC-based sources in an approach that ensures spectral compatibility with ensemble-based QMs. In addition, and regardless of the particular emitter chosen, it is important to better understand, and subsequently avoid or control spectral diffusion. This will enable multi-photon interference and in turn allow creating heralded entangled photons using four single photons as well as entanglement of qubits, also encoded into single rare-earth ions, over large distances.

- **Ensemble memories:** Owing to their large multimode storage capacity, long storage times, high fidelity and high storage efficiency, ensemble-based rare-earth memories have established themselves during the past 16 years as key systems for quantum repeaters. An important challenge for continued progress is to achieve all key requirements for quantum networks and repeaters with a single device. For instance, an ambitious yet reasonable goal would be a QM with ≥50% efficiency, ≥10 000 mode capacity, and ≥100 µs optical storage time with the possibility of extending the storage time to 100 ms through spin-wave storage. Other challenges include optimizing the entire memory system including cryostat and laser source to enable future field deployment. Towards this end, an interesting possibility is the creation of integrated (on-chip) devices following pioneering work in $Tm:LiNbO_3$[155] but exploiting the new waveguide fabrication possibilities that underpin the creation of nano-photonic cavities.

- **Individual qubits:** Over the past few years, the number of investigations related to interactions between photons and qubits encoded into individual rare-earth ions has increased rapidly, and qubit read-out as well as early stages of control and gate operations have been reported. This demonstrates that nano- and micro-cavity technology has reached the point where the limitations due to the long excited state lifetimes can be overcome and the benefits of these states for gate operations can finally be exploited. This work benefits from similar demonstrations with other emitters, including diamond vacancy centres and trapped atoms, that can be generalized conveniently to the new rare-earth systems. While interactions between rare-earth ions and surrounding lattice spins have been realized in a few groups, coupling between two (or more) rare-earth ions that enables controlled multi-qubit gates still remains to be demonstrated, an important goal for the near future. When such operations are available, it will become possible to progress to small processor nodes with a dense set of spectrally distinguishable qubits, in similarity with what has been achieved with spins in NV centres. But in comparison, a rare-earth processor node would offer better optical coherence as well as stronger ion–ion interactions, resulting in higher operation bandwidths and many more spectral channels.

Properties of rare-earth-ion doped crystals make them appealing and, due to their long optical coherence time, arguably unique candidates for light-matter interfaces needed in future quantum networks and especially in quantum repeaters. Recent progress towards the creation of three different network components, single photon emitters and long-lived qubits based on individual ions, as well as multi-mode QM for light based on large ensembles of ions. The fact that all of these can be based on the same material system

development of high-performance quantum networks. Indeed, the recent years have shown that exploring new operational regimes, different magnetic fields, doping concentrations etc, or new combinations of rare-earth ions and host crystals sometimes leads to better properties such as reduced sensitivity to environmental perturbations. The rich diversity of rare-earth systems is unique in this context, convinced to witness more, and more-advanced proof-of-principle demonstrations of quantum network technology, possibly including the first scalable quantum repeater, in the near future.

- **Data availability statement:** No new data were created or analysed in this study.
- **Acknowledgments:** This work has received funding from the Swiss State Secretariat for Education, Research and Innovation (SERI) under Contract Number UeM019-3 (W T and M A) and Contract Number UeM029-7 (MA). A K acknowledges support from the Wallenberg Centre for Quantum Technology (WACQT) funded by Knut and Alice Wallenberg Foundation (KAW). A W acknowledges support from the Swedish research council (Grant No. 2021-03755) and the Olle Engkvist Foundation.

ORCID iDs

- Wolfgang Tittel https://orcid.org/0000-0003-3136-8919
- Mikael Afzelius https://orcid.org/0000-0001-8367-6820
- Adam Kinos https://orcid.org/0000-0002-1472-0100

1. [Schrödinger E 1935 Discussion of probability relations between separated systems Math. Proc. Camb. Phil. Soc. 31 555] (https://doi.org/10.1017/S0305004100013554)
2. [Bell J S 1964 On the Einstein Podolsky Rosen paradox Physics 1 195] (https://doi.org/10.1103/PhysicsPhysiqueFizika.1.195)
3. [Aspect A, Grangier P and Roger G 1981 Experimental tests of realistic local theories via Bell's theorem Phys. Rev. Lett. 47 460] (https://doi.org/10.1103/PhysRevLett.47.460)
4. [Tittel W, Brendel J, Zbinden H and Gisin N 1998 Violation of Bell inequalities by photons more than 10 km apart Phys. Rev. Lett. 81 3563–6] (https://doi.org/10.1103/PhysRevLett.81.3563)
5. [Weihs G, Jennewein T, Simon C, Weinfurter H and Zeilinger A 1998 Violation of Bell's inequality under strict Einstein locality conditions Phys. Rev. Lett. 81 5039] (https://doi.org/10.1103/PhysRevLett.81.5039)
6. [Rowe M A, Kielpinski D, Meyer V, Sackett C A, Itano W M, Monroe C and Wineland D J 2001 Experimental violation of a Bell's inequality with efficient detection Nature 409 791] (https://doi.org/10.1038/35057215)
7. [Hensen B et al 2015 Loophole-free Bell inequality violation using electron spins separated by 1.3 kilometres Nature 526 682] (https://doi.org/10.1038/nature15759)
8. [Wehner S, Elkouss D and Hanson R 2018 Quantum internet: a vision for the road ahead Science 362 eaam9288] (https://doi.org/10.1126/science.aam9288)
9. [Gisin N, Ribordy G, Tittel W and Zbinden H 2002 Quantum cryptography Rev. Mod. Phys. 74 145] (https://doi.org/10.1103/RevModPhys.74.145)
10. [Van Meter R and Devitt S J 2016 The path to scalable distributed quantum computing IEEE Comput. 49 31] (https://doi.org/10.1109/MC.2016.291)
11. [Fitzsimons J F 2017 Private quantum computation: an introduction to blind quantum computing and related protocols npj Quantum Inf. 3 23] (https://doi.org/10.1038/s41534-017-0025-3)
12. [Guo X, Breum C, Borregaard J, Izumi S, Larsen M V, Gehring T, Christandl M, Beergard-Nielsen J S and Andersen I L 2020 Distributed quantum sensing in a continuous-variable entangled network Nat. Phys. 16 281] (https://doi.org/10.1038/s41567-019-0743-x)
13. [Kimble H J 2008 The quantum internet Nature 453 1023–30] (https://doi.org/10.1038/nature07127)
14. [Awschalom D D, Hanson R, Wrachtrup J and Zhou B 2018 Quantum technologies with optically interfaced solid-state spins Nat. Photon. 12 516–27] (https://doi.org/10.1038/s41566-018-0232-2)
15. [Reiserer A 2022 Colloquium: Cavity-enhanced quantum network nodes Rev. Mod. Phys. 94 041003] (https://doi.org/10.1103/RevModPhys.94.041003)
16. [Tomm N et al 2021 A bright and fast source of coherent single photons Nat. Nanotechnol. 16 399–403] (https://doi.org/10.1038/s41565-020-00831-x)
17. [Senellart P, Solomon G and White A 2017 High-performance semiconductor quantum-dot single-photon sources Nat. Nanotechnol. 12 1026–39] (https://doi.org/10.1038/nnano.2017.218)
18. [Zhang Q, Bao X-H, Lu C-Y, Zhou X-Q, Yang T, Rudolph T and Pan J-W 2008 Demonstration of a scheme for the generation of ‘event ready’ entangled photon pairs from a single photon source Phys. Rev. A 77 062316] (https://doi.org/10.1103/PhysRevA.77.062316)
19. [Cogan D, Su Z-E, Kenneth O and Gershoni D 2023 Deterministic generation of indistinguishable photons in a cluster state Nat. Photon. 17 324–9] (https://doi.org/10.1038/s41566-022-01152-2)
20. [Barrett S D and Kok P 2005 Efficient high-fidelity quantum computation using matter qubits and linear optics Phys. Rev. A 71 060310(R)] (https://doi.org/10.1103/PhysRevA.71.060310)
21. [Knaut C et al 2024 Entanglement of nanophotonic quantum memory nodes in a telecom network Nature 629 573–8] (https://doi.org/10.1038/s41586-024-07252-z)
22. [Bradley C E, Randall J, Abobeil M H, Berrevoets R C, Degen M J, Bakker M A, Markham M, Twitchen D J and Taminiau T H 2019 A ten-qubit solid-state spin register with quantum memory up to one minute Phys. Rev. X 9 031045] (https://doi.org/10.1103/PhysRevX.9
23. [Sanders B, Lvovsky A and Tittel W 2009 Optical quantum memory Nat. Photon. 3 706] (https://doi.org/10.1038/nphoton.200
24. [Briegel H-J, Dürr W, Cirac J I and Zoller P 1998 Quantum repeaters: the role of imperfect local operations in quantum communication Phys. Rev. Lett. 81 5932] (https://doi.org/10.1103/PhysRevLet
25. [Sangouard N, Simon C, De Riedmatten H and Gisin N 2011 Quantum repeaters based on atomic ensembles and linear optics Rev. Mod. Phys. 83 33] (https://doi.org/10.1103/RevModPhy
26. [Heshami K, England D G, Humphreys P C, Bustard P J, Acosta V M, Nunn J and Sussman B J 2016 Quantum memories: emerging applications and recent advances J. Mod. Opt. 63 2005] (https://doi.org/10.1080/09500340.2
27. [Zhong M, Hedges M P, Ahlefeld R L, Bartholomew J G, Beavan S E, Wittig S M, Longdell J J and Sellars M J 2015 Optically addressable nuclear spins in a solid with a six-hour coherence time Nature 517 7533] (https://doi.org/10.1038/nature1402
28. [Uysal T, Dusanowski L, Xu H, Horvarth S, Ourari S, Cava R, de Leon N and Thompson J 2024 Spin-photon entanglement of a single Er^{3+} ion in the telecom band (arXiv:2406.06497)] (https://arxiv.org/abs/2406.06497)
29. [Ruskuc A, Wu C-J, Green E, Hermans S, Choi J and Faraon A 2024 Scalable multipartite entanglement of remote rare-earth ion qubits (arXiv:2402.16224)] (https://arxiv.org/abs/2402.16224)
30. [Kinos A et al 2021 Roadmap for rare-earth quantum computing (arXiv:2103.15743)] (https://arxiv.org/abs/2103.15743)
31. [Dibos A M, Raha M, Phenicie C M and Thompson J D 2018 Atomic source of single photons in the telecom band Phys. Rev. Lett. 120 243601] (https://doi.org/10.1103/PhysRevLet

Rev. Lett. 121 183603] (https://doi.org/10.1103/PhysRevLett.121.183603)

33. [Chen S, Raha M, Phenicie C M, Ourari S and Thompson J D 2020 Parallel single-shot measurement and coherent control of solid-state spins below the diffraction limit Science 370 592–5] (https://doi.org/10.1126/science.abc7821)
34. [Ulanowski A, Merkel B and Reiserer A 2022 Spectral multiplexing of telecom emitters with stable transition frequency Sci. Adv. 8 eab04538] (https://doi.org/10.1126/sciadv.abo4538)
35. [Gritsch A, Ulanowski A and Reiserer A 2023 Purcell enhancement of single-photon emitters in silicon Optica 10 783–9] (https://doi.org/10.1364/OPTICA.486167)
36. [Deshmukh C, Beattie E, Casabone B, Grandi S, Serrano D, Ferrier A, Goldner P, Hunger D and de Riedmatten H 2023 Detection of single ions in a nanoparticle coupled to a fiber cavity Optica 10 1339–44] (https://doi.org/10.1364/OPTICA.489443)
37. [Yu Y, Oser D, Da Prato G, Urbinati E, Ávila J C, Zhang Y, Remy P, Marzban S, Gröblacher S and Tittel W 2023 Frequency tunable, cavity-enhanced single erbium quantum emitter in the telecom band Phys. Rev. Lett. 131 170801] (https://doi.org/10.1103/PhysRevLett.131.170801)
38. [Huang J-J, Liang P-J, Zheng L, Li P-Y, Ma Y-Z, Liu D-C, Xie J-H, Zhou Z-Q, Li C-F and Guo G-C 2023 Stark tuning of telecom single-photon emitters based on a single Er^{3+} Chin. Phys. Lett. 40 070301] (https://doi.org/10.1088/0256-307X/40/7/070301)
39. [Ourari S et al 2023 Indistinguishable telecom band photons from a single er ion in the solid state Nature 620 977–81] (https://doi.org/10.1038/s41586-023-06281-4)
40. [Yang L, Wang S, Shen M, Xie J and Tang H 2023 Controlling single rare earth ion emission in an electro-optical nanocavity Nat. Commun. 14 1718] (https://doi.org/10.1038/s41467-023-37513-w)

2012 Optical detection of a single rare-earth ion in a crystal Nat. Commun. 3 1029] (https://doi.org/10.1038/ncomms2034)

42. [Peev M et al 2009 The SECOQC quantum key distribution network in Vienna New J. Phys. 11 075001] (https://doi.org/10.1088/1367-2630/11/7/075001)
43. [Dynes J et al 2019 Cambridge quantum network npj Quantum Inf. 5 101] (https://doi.org/10.1038/s41534-019-0221-4)
44. [Chen T-Y et al 2021 Implementation of a 46-node quantum metropolitan area network npj Quantum Inf. 7 134] (https://doi.org/10.1038/s41534-021-00474-3)
45. [Chen Y-A et al 2021 An integrated space-to-ground quantum communication network over 4,600 kilometres Nature 589 214–9] (https://doi.org/10.1038/s41586-020-03093-8)
46. [For a network connecting 48 government organizations across Korea see (available at: www.idquantum.ie.com/idq-and-sk-broadband-complete-phase-one-of-nation-wide-korean-qkd-network/)] (https://www.idquantique.com/idq-and-sk-broadband-complete-phase-one-of-nation-wide-korean-qkd-network/)
47. [Lutkenhaus N, Calsamiglia J and Suominen K-A 1999 Bell measurements for teleportation Phys. Rev. A 59 3295] (https://doi.org/10.1103/PhysRevA.59.3295)
48. [Tittel W, Afzelius M, Chanelière T, Cone R L, Kröll S, Moiseev S A and Sellars M 2010 Photon-echo quantum memory in solid state systems Laser Photonics Rev. 4 244–67] (https://doi.org/10.1002/lpor.200810070)
49. [Bennett C H, Brassard G, Crépeau C, Jozsa R, Peres A and Wootters W K 1993 Teleporting an unknown quantum state via dual classical and Einstein-Podolsky-Rosen channels Phys. Rev. Lett. 70 1895] (https://doi.org/10.1103/PhysRevLett.70.1895)
50. [Sangouard N, Dubessy R and Simon C 2009 Quantum repeaters based on single trapped ions Phys. Rev. A 79 042340] (https://doi.org/10.1103/PhysRevA.79.042340)

1140–4] (https://doi.org/10.1126/science.aan

52. [Sinclair N et al 2014 Spectral multiplexing for scalable quantum photonics using an atomic frequency comb quantum memory and feed-forward control Phys. Rev. Lett. 113 053603] (https://doi.org/10.1103/PhysRevLet
53. [Michler M, Mattle K, Weinfurter H and Zeilinger A 1996 Interferometric Bell-state analysis Phys. Rev. A 53 1209(R)] (https://doi.org/10.1103/PhysRevA.5
54. [Grice W P 2011 Arbitrarily complete Bell-state measurement using only linear optical elements Phys. Rev. A 84 042331] (https://doi.org/10.1103/PhysRevA.8
55. [Bayerbach M J, D'Aurelio S E, van Loock P and Barz S 2023 Bell-state measurement exceeding 50% success probability with linear optics Sci. Adv. 9 eadf4080] (https://doi.org/10.1126/sciadv.adf4(
56. [Kinos A, Walther A, Kröll S and Rippe L 2023 Complete analysis of a realistic fiber-based quantum repeater scheme (arXiv:2309.04151 [quant-ph])] (https://arxiv.org/abs/2309.04151)
57. [Gu F, Menon S G, Maier D, Das A, Chakraborty T, Tittel W, Bernier H and Borregaard J 2024 Hybrid quantum repeaters with ensemble-based quantum memories and single-spin photon transducers (arXiv:2401.12395)] (https://arxiv.org/abs/2401.12395)
58. [Equall R W, Cone R L and Macfarlane R M 1995 Homogeneous broadening and hyperfine structure of optical transitions in Pr^{3+}:Y_2SiO_5 Phys. Rev. B 52 3963–9] (https://doi.org/10.1103/PhysRevB.5
59. [Yano R, Mitsunaga M and Uesugi N 1992 Nonlinear laser spectroscopy of Eu^{3+}:Y_2SiO_5 and its application to time-domain optical memory J. Opt. Soc. Am. B 9 992–7] (https://doi.org/10.1364/JOSAB.9.00
60. [Thiel C W, Sun Y, Böttger T, Babbitt W R and Cone R L 2010 Optical decoherence and persistent spectral hole burning in Tm^{3+}:$LiNbO_3$ J. Lumin. 130 1598–602] (https://doi.org/10.1016/j.jlumin.201(

states of Eu^{3+}:Y_2SiO_5 Phys. Rev. B 77 085124] (https://doi.org/10.1103/PhysRevB.77.085124)

62. [Rančić M, Hedges M P, Ahlefeldt R L and Sellars M J 2017 Coherence time of over a second in a telecom-compatible quantum memory storage material Nat. Phys. 14 50–54] (https://doi.org/10.1038/nphys4254)
63. [Ortu A, Tiranov A, Welinski S, Fröwis F, Gisin N, Ferrier A, Goldner P and Afzelius M 2018 Simultaneous coherence enhancement of optical and microwave transitions in solid-state electronic spins Nat. Mater. 17 671–5] (https://doi.org/10.1038/s41563-018-0116-2)
64. [Equall R W, Sun Y, Cone R L and Macfarlane R M 1994 Ultraslow optical dephasing in Eu^{3+}:Y_2SiO_5 Phys. Rev. Lett. 72 2179] (https://doi.org/10.1103/PhysRevLett.72.2179)
65. [Böttger T, Thiel C W, Cone R L and Sun Y 2009 Effects of magnetic field orientation on optical decoherence in Er^{3+}:Y_2SiO_5 Phys. Rev. B 79 115104] (https://doi.org/10.1103/PhysRevB.79.115104)
66. [Falamarzi Askarani M et al 2021 Long-lived solid-state optical memory for high-rate quantum repeaters Phys. Rev. Lett. 127 220502] (https://doi.org/10.1103/PhysRevLett.127.220502)
67. [Könz F, Sun Y, Thiel C W, Cone R L, Equall R W, Hutcheson R L and Macfarlane R L 2003 Temperature and concentration dependence of optical dephasing, spectral-hole lifetime and anisotropic absorption in Eu^{3+}:Y_2SiO_5 Phys. Rev. B 68 085109] (https://doi.org/10.1103/PhysRevB.68.085109)
68. [Oswald R, Hansen M G, Wiens E, Nevsky A Y and Schiller S 2018 Characteristics of long-lived persistent spectral holes in Eu^{3+}:Y_2SiO_5 at 1.2 K Phys. Rev. A 98 062516] (https://doi.org/10.1103/PhysRevA.98.062516)
69. [Thiel C W, Böttger T and Cone R L 2011 Rare-earth-doped materials for applications in quantum information storage and signal processing J. Lumin. 131 353–61] (https://doi.org/10.1016/j.jlumin.2010.12.015)

processing Handbook on the Physics and Chemistry of Rare Earths (Elsevier) pp 1–78] (https://doi.org/10.1016/B978-0-444-63260-9.00267-4)

71. [Hull R, Parisi J, Osgood R, Warlimont H, Liu G and Jacquier B 2005 Spectroscopic Properties of Rare Earths in Optical Materials (Springer)] (https://doi.org/10.1007/3-540-28209-2)
72. [Burnham D C and Weinberg D L 1970 Observation of simultaneity in parametric production of optical photon pairs Phys. Rev. Lett. 25 84] (https://doi.org/10.1103/PhysRevLett.25.84)
73. [Ou Z Y and Mandel L 1988 Violation of Bell's inequality and classical probability in a two-photon correlation experiment Phys. Rev. Lett. 61 50] (https://doi.org/10.1103/PhysRevLett.61.50)
74. [Giustina M et al 2015 Significant-loophole-free test of Bell's theorem with entangled photons Phys. Rev. Lett. 115 250401] (https://doi.org/10.1103/PhysRevLett.115.250401)
75. [Shalm L K et al 2015 Strong loophole-free test of local realism Phys. Rev. Lett. 115 250402] (https://doi.org/10.1103/PhysRevLett.115.250402)
76. [Jennewein T, Simon G, Weihs G, Weinfurter H and Zeilinger A 2000 Quantum cryptography with entangled photons Phys. Rev. Lett. 84 4729] (https://doi.org/10.1103/PhysRevLett.84.4729)
77. [Naik D S, Peterson C G, White A G, Berglund A G and Kwiat P G 2000 Entangled state quantum cryptography: eavesdropping on the ekert protocol Phys. Rev. Lett. 84 4733] (https://doi.org/10.1103/PhysRevLett.84.4733)
78. [Tittel W, Brendel J, Zbinden H and Gisin N 2000 Quantum cryptography using entangled photons in energy-time Bell states Phys. Rev. Lett. 84 4737] (https://doi.org/10.1103/PhysRevLett.84.4737)
79. [Bouwmeester D, Pan J-W, Mattle K, Eibl M, Weinfurter H and Zeilinger A 1997 Experimental quantum teleportation Nature 390 575] (https://doi.org/10.1038/37539)

teleporting an unknown pure quantum state via dual classical and Einstein-Podolsky-Rosen channels Phys. Rev. Lett. 80 1121] (https://doi.org/10.1103/PhysRevLet

81. [Valivarthi R, Puigibert M I G, Zhou Q, Aguilar G H, Verma V B, Marsili F, Shaw M D, Nam S W, Oblak D and Tittel W 2016 Quantum teleportation across a metropolitan fibre network Nat. Photon. 10 676–80] (https://doi.org/10.1038/nphoton.201
82. [Sun Q-C et al 2016 Quantum teleportation with independent sources and prior entanglement distribution over a network Nat. Photon. 10 671] (https://doi.org/10.1038/nphoton.201
83. [Ma X et al 2012 Quantum teleportation over 143 kilometres using active feed-forward Nature 489 269] (https://doi.org/10.1038/nature1147
84. [Ren J-G et al 2017 Ground-to-satellite quantum teleportation Nature 549 70] (https://doi.org/10.1038/nature2367
85. [Guha S, Krovi H, Fuchs C A, Dutton Z, Slater J A, Simon C and Tittel W 2015 Rate-loss analysis of an efficient quantum repeater architecture Phys. Rev. A 92 022357] (https://doi.org/10.1103/PhysRevA.9
86. [Pirandola S, Laurenza R, Ottaviani C and Banchi L 2017 Fundamental limits of repeaterless quantum communications Nat. Commun. 8 15043] (https://doi.org/10.1038/ncomms150
87. [Takeoka M, Guha S and Wilde M M 2014 Fundamental rate-loss tradeoff for optical quantum key distribution Nat. Commun. 5 5235] (https://doi.org/10.1038/ncomms623
88. [Reiserer A, Ritter S and Rempe G 2013 Nondestructive detection of an optical photon Science 342 1379] (https://doi.org/10.1126/science.124
89. [Sinclair N, Heshami K, Deshmukh C, Oblak D, Simon C and Tittel W 2016 Proposal and proof-of-principle demonstration of non-destructive detection of photonic qubits using a Tm:$LiNbO_3$ waveguide Nat. Commun. 7 13454] (https://doi.org/10.1038/ncomms134

parametric down-conversion sources Appl. Phys. B 122 52] (https://doi.org/10.1007/s00340-015-6297-4)

91. [Huang Y-P and Kumar P 2012 Antibunched emission of photon pairs via quantum zeno blockade Phys. Rev. Lett. 108 030502] (https://doi.org/10.1103/PhysRevLett.108.030502)
92. [Franson J D 1989 Bell inequality for position and time Phys. Rev. Lett. 62 2205] (https://doi.org/10.1103/PhysRevLett.62.2205)
93. [Huber D, Reindl M, Aberl J, Rastelli A and Trotta A 2018 Semiconductor quantum dots as an ideal source of polarization-entangled photon pairs on-demand: a review J. Opt. 20 073002] (https://doi.org/10.1088/2040-8986/aac62b)
94. [Browne D E and Rudolph T 2005 Resource-efficient linear optical quantum computation Phys. Rev. Lett. 95 010501] (https://doi.org/10.1103/PhysRevLett.95.010501)
95. [Bogdanov S I et al 2018 Ultrabright room-temperature sub-nanosecond emission from single nitrogen-vacancy centers coupled to nanopatch antennas Nano Lett. 18 4837–44] (https://doi.org/10.1021/acs.nanolett.8b01415)
96. [Ruf M, Weaver M J, van Dam S B and Hanson R 2021 Resonant excitation and purcell enhancement of coherent nitrogen-vacancy centers coupled to a Fabry-Perot microcavity Phys. Rev. Appl. 15 024049] (https://doi.org/10.1103/PhysRevApplied.15.024049)
97. [Pelton M 2015 Modified spontaneous emission in nanophotonic structures Nat. Photon. 9 427–35] (https://doi.org/10.1038/nphoton.2015.103)
98. [Khriachtchev L 2016 Silicon Nanophotonics. Basic Principles, Present Status and Perspectives (Jenny Stanford Publishing)] (https://doi.org/10.1201/9781315364797)
99. [Istrate E and Sargent E H 2006 Photonic crystal heterostructures and interfaces Rev. Mod. Phys. 78 455–80] (https://doi.org/10.1103/RevModPhys.78.455)
100. [Burek M J, Chu Y, Liddy M S Z, Patel P, Rochman J, Meesala S, Hong W, Quan Q, Lukin M D and Loncar M 2014 High quality-factor optical nanocavities in bulk single-crystal diamond Nat. Commun. 5 5718] (https://doi.org/10.1038/ncomms6718)

microdisks fabricated with quasi-isotropic etching Nano Lett. 15 5131–6] (https://doi.org/10.1021/acs.nanolett.5b01346)

102. [Zhong T, Rochman J, Kindem J M, Miyazono E and Faraon A 2016 High quality factor nanophotonic resonators in bulk rare-earth doped crystals Opt. Express 24 536–44] (https://doi.org/10.1364/OE.24.000536)
103. [Rüsing M, Weigel P O, Zhao J and Mookherjea S 2019 Toward 3D integrated photonics including lithium niobate thin films IEEE Nanotechnol. Mag. 13 18–33] (https://doi.org/10.1109/MNANO.2019.2916115)
104. [Li M, Liang H, Luo R, He Y, Ling J and Lin Q 2019 Photon-level tuning of photonic nanocavities Optica 6 860–3] (https://doi.org/10.1364/OPTICA.6.000860)
105. [Boes A, Corcoran B, Chang L, Bowers J and Mitchell A 2018 Status and potential of lithium niobate on insulator (LNOI) for photonic integrated circuits Laser Photonics Rev. 12 1700256] (https://doi.org/10.1002/lpor.201700256)
106. [Li Z et al 2023 High density lithium niobate photonic integrated circuits Nat. Commun. 14 4856] (https://doi.org/10.1038/s41467-023-40502-8)
107. [Hunger D, Steinmetz T, Colombe Y, Deutsch C, Hänsch T W and Reichel J 2010 A fiber Fabry–Perot cavity with high finesse New J. Phys. 12 065038] (https://doi.org/10.1088/1367-2630/12/6/065038)
108. [Ortu A, Holzapfel A, Etesse J and Afzelius M 2022 Storage of photonic time-bin qubits for up to 20 ms in a rare-earth doped crystal npj Quantum Inf. 8 29] (https://doi.org/10.1038/s41534-022-00541-3)
109. [Duranti S, V Wengerowsky S, Feldmann L, Seri A, Casabone B and De Riedmatten H 2024 Efficient cavity-assisted storage of photonic qubits in a solid-state quantum memory Opt. Express 32 26884] (https://doi.org/10.1364/OE.489318)

Afzelius M 2022 Non-classical correlations over 1250 modes between telecom photons and 979-nm photons stored in $^{171}Yb^{3+}:Y_2SiO_5$ Nat. Commun. 13 6438] (https://doi.org/10.1038/s41467-022-34158-2)

111. [Tanzilli S, Tittel W, Halder M, Alibart O, Baldi P, Gisin N and Zbinden H 2005 A photonic quantum information interface Nature 437 116–20] (https://doi.org/10.1038/nature0400
112. [Dréau A, Tchebotareva A, El Mahdaoui A, Bonato C and Hanson R 2018 Quantum frequency conversion of single photons from a nitrogen-vacancy center in diamond to telecommunication wavelengths Phys. Rev. Appl. 9 064031] (https://doi.org/10.1103/PhysRevAp
113. [Maring N, Lago-Rivera D, Lenhard A, Heinze G and De Riedmatten H 2018 Quantum frequency conversion of memory-compatible single photons from 606 nm to the telecom C-band Optica 5 507–13] (https://doi.org/10.1364/OPTICA.5.0
114. [Merkel B, Ulanowski A and Reiserer A 2020 Coherent and purcell-enhanced emission from erbium dopants in a cryogenic high-Q resonator Phys. Rev. X 10 041025] (https://doi.org/10.1103/PhysRevX.1
115. [Xia K et al 2022 Tunable microcavities coupled to rare-earth quantum emitters Optica 9 445–50] (https://doi.org/10.1364/OPTICA.45
116. [Dutta S, Zhao Y, Saha U, Farfurnik D, Goldschmidt E A and Waks E 2023 An atomic frequency comb memory in rare-earth-doped thin-film lithium niobate ACS Photonics 10 1104–9] (https://doi.org/10.1021/acsphotonic
117. [Kindem J M, Ruskuc A, Bartholomew J G, Rochman J, Huan Y Q and Faraon A 2020 Control and single-shot readout of an ion embedded in a nanophotonic cavity Nature 580 201] (https://doi.org/10.1038/s41586-020-2160-8)
118. [Simon C, De Riedmatten H, Afzelius M, Sangouard N, Zbinden H and Gisin N 2007 Quantum repeaters with photon pair sources and multimode memories Phys. Rev. Lett. 98 190503] (https://doi.org/10.1103/PhysRevLet

memories in atomic ensembles Phys. Rev. Lett. 101 260502] (https://doi.org/10.1103/PhysRevLett.101.260502)

120. [Afzelius M, Simon C, de Riedmatten H and Gisin N 2009 Multimode quantum memory based on atomic frequency combs Phys. Rev. A 79 052329] (https://doi.org/10.1103/PhysRevA.79.052329)
121. [Ortu A, Rakonjac J V, Holzapfel K, Seri A, Grandi S, Mazzera M, de Riedmatten H and Afzelius M 2022 Multimode capacity of atomic-frequency comb quantum memories Quantum Sci. Technol. 7 035024] (https://doi.org/10.1088/2058-9565/ac6b8c)
122. [Abella J D, Kurnit N A and Hartmann S R 1966 Photon echoes Phys. Rev. 141 391–406] (https://doi.org/10.1103/PhysRev.141.391)
123. [Jobez P, Usmani I, Laplane C, Gisin N and Afzelius M 2016 Towards highly multimode optical quantum memory for quantum repeaters Phys. Rev. A 93 032327] (https://doi.org/10.1103/PhysRevA.93.032327)
124. [Businger M, Nicolas L, Mejia T S, Ferrier A, Goldner P and Afzelius M 2022 Non-classical correlations over 1250 modes between telecom photons and 979-nm photons stored in $^{171}Yb^{3+}$:Y_3SiO_5 Nat. Commun. 13 6438] (https://doi.org/10.1038/s41467-022-34158-2)
125. [Sangouard N, Simon C, Afzelius M and Gisin N 2007 Analysis of a quantum memory for photons based on controlled reversible inhomogeneous broadening Phys. Rev. A 75 032327] (https://doi.org/10.1103/PhysRevA.75.032327)
126. [Gorshkov A V, André A, Lukin M D and Sørensen A S 2007 Photon storage in Λ-type optically dense atomic media. II. Free-space model Phys. Rev. A 76 033805] (https://doi.org/10.1103/PhysRevA.76.033805)
127. [Afzelius M and Simon C 2010 Impedance-matched cavity quantum memory Phys. Rev. A 82 022310] (https://doi.org/10.1103/PhysRevA.82.022310)
128. [Jöbez P, Usmani I, Timoney N, Gisin N, Ferrier A, Goldner P and Afzelius M 2014 Cavity-enhanced storage in an optical spin-wave memory New J. Phys. 16 083005] (https://doi.org/10.1088/1367-2630/16/8/083005)
129. [Afzelius M et al 2010 Demonstration of atomic frequency comb memory for light with spin-wave storage Phys. Rev. Lett. 104 040503] (https://doi.org/10.1103/PhysRevLett.104.040503)
130. [Kraus B, Tittel W, Gisin N, Nilsson M, Kröll S and Cirac J I 2006 Quantum memory for nonstationary light fields based on controlled reversible inhomogeneous broadening Phys. Rev. A 73 020302] (https://doi.org/10.1103/PhysRevA.73.020302)
131. [Alexander A L, Longdell J J, Sellars M J and Manson N B 2006 Photon echoes produced by switching electric fields Phys. Rev. Lett. 96 043602-4] (https://doi.org/10.1103/PhysRevLett.96.043602)
132. [Damon V, Bonarota M, Louchet-Chauvet A, Chanelière T and Gouët J-L L 2011 Revival of silenced echo and quantum memory for light New J. Phys. 13 093031-] (https://doi.org/10.1088/1367-2630/13/9/093031)
133. [Bonarota M, Gouët J-L L and Chanelière T 2014 Photon echo with a few photons in two-level atoms Laser Phys. 24 094003] (https://doi.org/10.1088/1054-660X/24/9/094003)
134. [Ma Y-Z, Jin M, Chen D-L, Zhou Z-Q, Li C-F and Guo G-C 2021 Elimination of noise in optically rephased photon echoes Nat. Commun. 12 4378] (https://doi.org/10.1038/s41467-021-24680-5)
135. [Nicolas L, Businger M, Sanchez Mejia K, Tiranov A, Chanelière T, Lafitte-Houssat E, Ferrier A, Goldner P and Afzelius M 2023 Coherent optical-microwave interface for manipulation of low-field electronic clock transitions in $^{171}Yb^{3+}$:Y_3SiO_5 npj Quantum Inf. 9 21] (https://doi.org/10.1038/s41534-023-00683-y)
136. [Horvath S P, Algedra M K, Kinos A, Walther A, Dahlström J M, Kröll S and Rippe L 2021 Noise-free on-demand atomic frequency comb quantum memory Phys. Rev. Res. 3 023099] (https://doi.org/10.1103/PhysRevResearch.3.023099)
137. [Minář J C V, Sangouard N, Afzelius M, de Riedmatten H and Gisin N 2010 Spin-wave storage using chirped control fields in atomic frequency comb-based quantum memory Phys. Rev. A 82 042309] (https://doi.org/10.1103/PhysRevA.82.042309)
138. [Chen J and Afzelius M 2024 Efficient and reversible optical-to-spin conversion for solid-state quantum memories (arXiv:2410.14551)] (https://arxiv.org/abs/2410.14551)
139. [Gündoğan M, Ledingham P M, Kutluer K, Mazzera M and de Riedmatten H 2015 Solid state spin-wave quantum memory for time-bin qubits Phys. Rev. Lett. 114 230501] (https://doi.org/10.1103/PhysRevLet
140. [Jöbez P, Laplane C, Timoney N, Gisin N, Ferrier A, Goldner P and Afzelius M 2015 Coherent spin control at the quantum level in an ensemble-based optical memory Phys. Rev. Lett. 114 230502] (https://doi.org/10.1103/PhysRevLet
141. [Holzapfel A, Etesse J, Kaczmarek K T, Tiranov A, Gisin N and Afzelius M 2020 Optical storage for 0.53 s in a solid-state atomic frequency comb memory using dynamical decoupling New J. Phys. 22 063009] (https://doi.org/10.1088/1367-2630/ab8ff4)
142. [Ledingham P M, Naylor W R, Longdell J J, Beavan S E and Sellars M J 2010 Nonclassical photon streams using rephased amplified spontaneous emission Phys. Rev. A 81 012301] (https://doi.org/10.1103/PhysRevA.8
143. [Sekatski P, Sangouard N, Gisin N, de Riedmatten H and Afzelius M 2011 Photon-pair source with controllable delay based on shaped inhomogeneous broadening of rare-earth-metal-doped solids Phys. Rev. A 83 053840] (https://doi.org/10.1103/PhysRevA.8
144. [Hain M, Stabel M and Halfmann T 2022 Few-photon storage on a second timescale by electromagnetically induced transparency in a doped solid New J. Phys. 24 023012] (https://doi.org/10.1088/1367-2630/ac4b13)

ensemble-based quantum memories Phys. Rev. A 101 042301] (https://doi.org/10.1103/PhysRevA.101.042301)

148. [Staudt M U, Afzelius M, de Riedmatten H, Hastings-Simon S R, Simon C, Ricken R, Suche H, Sohler W and Gisin N 2007 Interference of multimode photon echoes generated in spatially separated solid-state atomic ensembles Phys. Rev. Lett. 99 173602] (https://doi.org/10.1103/PhysRevLett.99.173602)
149. [de Riedmatten H, Afzelius M, Staudt M U, Simon C and Gisin N 2008 A solid-state light-matter interface at the single-photon level Nature 456 773-7] (https://doi.org/10.1038/nature07607)
150. [Zhou Z-Q, Lin W-B, Yang M, Li C-F and Guo G-C 2012 Realization of reliable solid-state quantum memory for photonic polarization qubit Phys. Rev. Lett. 108 190505] (https://doi.org/10.1103/PhysRevLett.108.190505)
151. [Rakonjac J V, Lago-Rivera D, Mazzera M, Grandi S, Osellame R and de Riedmatten H 2021 Entanglement between a telecom photon and an on-demand multimode solid-state quantum memory Phys. Rev. Lett. 127 210502] (https://doi.org/10.1103/PhysRevLett.127.210502)
152. [Jin M, Ma Y-Z, Zhou Z-Q, Li C-F and Guo G-C 2022 A faithful solid-state spin-wave quantum memory for polarization qubits Sci. Bull. 67 676-8] (https://doi.org/10.1016/j.scib.2022.01.019)
153. [Arnold N T, Victora M, Goggin M E and Kwiat P G 2023 Free-space photonic quantum memory Proc. SPIE 12446 1244606] (https://doi.org/10.1117/12.2650039)
154. [Clausen C, Usmani I, Bussieres F, Sangouard N, Afzelius M, de Riedmatten H and Gisin N 2011 Quantum storage of photonic entanglement in a crystal Nature 469 508-11] (https://doi.org/10.1038/nature09662)
155. [Saglamyurek E, Sinclair N, Jin J, Slater J A, Oblak D, Bussieres F, George M, Ricken R, Sohler W and Tittel W 2011 Broadband waveguide quantum memory for entangled photons Nature 469 512-5] (https://doi.org/10.1038/nature09719)
157. [Etesse J, Holzapfel A, Ortu A and Afzelius M 2021 Optical and spin manipulation of non-kramers rare-earth ions in a weak magnetic field for quantum memory applications Phys. Rev. A 103 022618] (https://doi.org/10.1103/PhysRevA.103.022618)
158. [Wei S-H et al 2024 Quantum storage of 1650 modes of single photons at telecom wavelength npj Quantum Inf. 10 19] (https://doi.org/10.1038/s41534-024-00809-w)
159. [Rakonjac J V, Corrielli G, Lago-Rivera D, Seri A, Mazzera M, Grandi S, Osellame R and de Riedmatten H 2022 Storage and analysis of light-matter entanglement in a fiber-integrated system Sci. Adv. 8 eabn3919] (https://doi.org/10.1126/sciadv.abn3919)
160. [Craiciu I, Lei M, Rochman J, Kindem J M, Bartholomew J G, Miyazono E, Zhong T, Sinclair N and Faraon A 2019 Nanophotonic quantum storage at telecommunication wavelength Phys. Rev. Appl. 12 024062] (https://doi.org/10.1103/PhysRevApplied.12.024062)
161. [Ma Y, Ma Y-Z, Zhou Z-Q, Li C-F and Guo G 2021 One-hour coherent optical storage in an atomic frequency comb memory Nat. Commun. 12 2381] (https://doi.org/10.1038/s41467-021-22706-y)
162. [Saglamyurek E, Jin J, Verma V B, Shaw M D, Marsili F, Nam S W, Oblak D and Tittel W 2015 Quantum storage of entangled telecom-wavelength photons in an erbium-doped optical fibre Nat. Photon. 9 83-87] (https://doi.org/10.1038/nphoton.2014.311)
163. [Clausen C, Bussières F, Afzelius M and Gisin N 2012 Quantum storage of heralded polarization qubits in birefringent and anisotropically absorbing materials Phys. Rev. Lett. 108 190503] (https://doi.org/10.1103/PhysRevLett.108.190503)
164. [Gündoğan M, Ledingham P M, Almasi A, Cristiani M and de Riedmatten H 2012 Quantum storage of a photonic polarization qubit in a solid Phys. Rev. Lett. 108 190504] (https://doi.org/10.1103/PhysRevLett.108.190504)
166. [Tiranov A et al 2015 Storage of hyperentanglement in a solid-state quantum memory Optica 2 279–87] (https://doi.org/10.1364/OPTICA.2.0
167. [Bussières F et al 2014 Quantum teleportation from a telecom-wavelength photon to a solid-state quantum memory Nat. Photon. 8 775–8] (https://doi.org/10.1038/nphoton.201
168. [Lago-Rivera D, Rakonjac J V, Grandi S and Riedmatten H d 2023 Long distance multiplexed quantum teleportation from a telecom photon to a solid-state qubit Nat. Commun. 14 1889] (https://doi.org/10.1038/s41467-023-37499-3)
169. [Iuliano M et al 2024 Qubit teleportation between a memory-compatible photonic time-bin qubit and a solid-state quantum network node (arXiv:2403.18581)] (https://arxiv.org/abs/2403.18581)
170. [Liu X et al 2024 Nonlocal photonic quantum gates over 7.0 km Nat. Commun. 15 8529] (https://doi.org/10.1038/s41467-024-52913-9)
171. [Rakonjac J V, Grandi S, Wengerowsky S, Lago-Rivera D, Appas F and de Riedmatten H 2023 Transmission of light–matter entanglement over a metropolitan network Opt. Quantum 1 94] (https://doi.org/10.1038/s41534-023-00668-x)
172. [Usmani I, Clausen C, Bussières F, Sangouard N, Afzelius M and Gisin N 2012 Heralded quantum entanglement between two crystals Nat. Photon. 6 234] (https://doi.org/10.1038/nphoton.201
173. [Grimau Puigibert M, Askarani M F, Davidson J H, Verma V B, Shaw M D, Nam S W, Lutz T, Amaral G C, Oblak D and Tittel W 2020 Entanglement and nonlocality between disparate solid-state quantum memories mediated by photons Phys. Rev. Res. 2 013039] (https://doi.org/10.1103/PhysRevRe

heralded entanglement between multimode solid-state quantum memories Nature 594 37–40] (https://doi.org/10.1038/s41586-021-03481-8)

175. [Liu X, Hu J, Li Z-F, Li X, Li P-Y, Liang P-J, Zhou Z-Q, Li C-F and Guo G-C 2021 Heralded entanglement distribution between two absorptive quantum memories Nature 594 41–45] (https://doi.org/10.1038/s41586-021-03505-3)
176. [Usmani I, Afzelius M, de Riedmatten H and Gisin N 2010 Mapping multiple photonic qubits into and out of one solid-state atomic ensemble Nat. Commun. 1 1–7] (https://doi.org/10.1038/ncomms1010)
177. [Tang J-S et al 2015 Storage of multiple single-photon pulses emitted from a quantum dot in a solid-state quantum memory Nat. Commun. 6 8652] (https://doi.org/10.1038/ncomms9652)
178. [Bonarota M, Gouët J-L L and Chanelière T 2011 Highly multimode storage in a crystal New J. Phys. 13 013013] (https://doi.org/10.1088/1367-2630/13/1/013013)
179. [Zhou Z-Q, Hua Y-L, Liu X, Chen G, Xu J-S, Han Y-J, Li C-F and Guo G-C 2015 Quantum storage of three-dimensional orbital-angular-momentum entanglement in a crystal Phys. Rev. Lett. 115 070502] (https://doi.org/10.1103/PhysRevLett.115.070502)
180. [Seri A, Lago-Rivera D, Lenhard A, Corrielli G, Osellame R, Mazzera M and de Riedmatten H 2019 Quantum storage of frequency-multiplexed heralded single photons Phys. Rev. Lett. 123 080502] (https://doi.org/10.1103/PhysRevLett.123.080502)
181. [Yang T-S et al 2018 Multiplexed storage and real-time manipulation based on a multiple degree-of-freedom quantum memory Nat. Commun. 9 3407] (https://doi.org/10.1038/s41467-018-05669-5)
182. [Amari A et al 2010 Towards an efficient atomic frequency comb quantum memory J. Lumin. 130 1579–85] (https://doi.org/10.1016/j.jlumin.2010.03.032)
183. [Afzelius M, Usmani I, Amari A, Lauritzen B, Walther A, Simon C, Sangouard N, Minář J, de Riedmatten H, Gisin N, Kröll S 2010 Demonstration of atomic frequency comb memory for light with spin-wave storage Phys. Rev. Lett. 104 040503] (https://doi.org/10.1103/PhysRevLett.104.040503)
184. [Davidson J H, Lefebvre P, Zhang J, Oblak D and Tittel W 2020 Improved light-matter interaction for storage of quantum states of light in a thulium-doped crystal cavity Phys. Rev. A 101 042333] (https://doi.org/10.1103/PhysRevA.101.042333)
185. [Hedges M P, Longdell J J, Li Y and Sellars M J 2010 Efficient quantum memory for light Nature 465 1052–6] (https://doi.org/10.1038/nature09081)
186. [Ferguson K R, Beavan S E, Longdell J J and Sellars M J 2016 Generation of light with multimode time-delayed entanglement using storage in a solid-state spin-wave quantum memory Phys. Rev. Lett. 117 020501] (https://doi.org/10.1103/PhysRevLett.117.020501)
187. [Duda C K, Ferguson K R, Ahlefeldt R L, Hedges M P and Sellars M J 2023 Optimizing the efficiency of a quantum memory based on rephased amplified spontaneous emission Phys. Rev. A 107 L030602] (https://doi.org/10.1103/PhysRevA.107.L030602)
188. [Stuart J, Smith K, Hedges M, Ahlefeldt R and Sellars M 2024 Progress towards efficient 4-level photon echo memories (arXiv:2409.12503)] (https://arxiv.org/abs/2409.12503)
189. [Laplane C, Jobez P, Etesse J, Gisin N and Afzelius M 2017 Multimode and long-lived quantum correlations between photons and spins in a crystal Phys. Rev. Lett. 118 210501] (https://doi.org/10.1103/PhysRevLett.118.210501)
190. [Kutluer K, Mazzera M and de Riedmatten H 2017 Solid-state source of nonclassical photon pairs with embedded multimode quantum memory Phys. Rev. Lett. 118 210502] (https://doi.org/10.1103/PhysRevLett.118.210502)
191. [Kutluer K, Distante E, Casabone B, Duranti S, Mazzera M and de Riedmatten H 2019 Time entanglement between a photon and a spin wave in a multimode solid-state quantum memory Phys. Rev. Lett. 123 030501] (https://doi.org/10.1103/PhysRevLett.123.030501)
193. [Stuart J S, Hedges M, Ahlefeldt R and Sellars M 2021 Initialization protocol for efficient quantum memories using resolved hyperfine structure Phys. Rev. Res. 3 1032054] (https://doi.org/10.1103/PhysRevRe
194. [Askarani M F, Puigibert M G, Lutz T, Verma V B, Shaw M D, Nam S W, Sinclair N, Oblak D and Tittel W 2019 Storage and reemission of heralded telecommunication-wavelength photons using a crystal waveguide Phys. Rev. Appl. 11 054056] (https://doi.org/10.1103/PhysRevAp
195. [Zhang X et al 2023 Telecom-band integrated multimode photonic quantum memory Sci. Adv. 9 eadf4587] (https://doi.org/10.1126/sciadv.adf45
196. [Jiang M-H, Xue W, He Q, An Y-Y, Zheng X, Xu W-J, Xie Y-B, Lu Y, Zhu S and Ma X-S 2023 Quantum storage of entangled photons at telecom wavelengths in a crystal Nat. Commun. 14 6995] (https://doi.org/10.1038/s41467-023-42741-1)
197. [Staudt M U, Hastings-Simon S R, Afzelius M, Jaccard D, Tittel W and Gisin N 2006 Investigations of optical coherence properties in an erbium-doped silicate fiber for quantum state storage Opt. Commun. 266 720–6] (https://doi.org/10.1016/j.optcom.20
198. [Hastings-Simon S R, Lauritzen B, Staudt M U, van Mechelen J L M, Simon C, de Riedmatten H, Afzelius M and Gisin N 2008 Zeeman-level lifetimes in Er^{3+}:Y_2SiO_5 Phys. Rev. B 78 085410] (https://doi.org/10.1103/PhysRevB.7
199. [Lauritzen B, Hastings-Simon S R, de Riedmatten H, Afzelius M and Gisin N 2008 State preparation by optical pumping in erbium-doped solids using stimulated emission and spin mixing Phys. Rev. A 78 043402] (https://doi.org/10.1103/PhysRevA.7
200. [Ohlsson N, Mohan K and Kroll S 2002 Quantum computer hardware based on rare-earth-ion-doped inorganic crystals Opt. Commun. 201 1–3] (https://doi.org/10.1016/S0030-4018(01)01666-2)

and Schmidt-Kaler F 2019 Deterministic single-ion implantation of rare-earth ions for nanometer-resolution color-center generation Phys. Rev. Lett. 123 106802] (https://doi.org/10.1103/PhysRevLett.123.106802)

202. [Kinos A, Rippe L, Kröll S and Walther A 2021 Designing gate operations for single ion quantum computing in rare-earth-ion-doped crystals Phys. Rev. A 104 052624] (https://doi.org/10.1103/PhysRevA.104.052624)
203. [Kinos A, Rippe L, Walther A and Kröll S 2022 Microscopic treatment of instantaneous spectral diffusion and its effect on quantum gate fidelities in rare-earth-ion-doped crystals Phys. Rev. A 105 032608] (https://doi.org/10.1103/PhysRevA.105.032608)
204. [Preskill J 2018 Quantum computing in the NISQ era and beyond Quantum 2 79] (https://doi.org/10.22331/q-2018-08-06-79)
205. [Walther A, Julsgaard B, Rippe L, Ying Y and Kröll S 2009 Extracting high fidelity quantum computer hardware from random systems Phys. Scr. T137 014009] (https://doi.org/10.1088/0031-8949/2009/T137/014009)
206. [Wesenberg J, Molmer K, Rippe L and Kröll S 2007 Scalable designs for quantum computing with rare-earth-ion-doped crystals Phys. Rev. A 75 012304] (https://doi.org/10.1103/PhysRevA.75.012304)
207. [Kimiaee Asadi F, Lauk N, Wein S, Sinclair N, O'Brien C and Simon C 2018 Quantum repeaters with individual rare-earth ions at telecommunication wavelengths Quantum 2 93] (https://doi.org/10.22331/q-2018-09-13-93)
208. [Debnath K, Kiilerich A H and Mølmer K 2021 Ancilla-mediated qubit readout and heralded entanglement between rare-earth dopant ions in crystals Phys. Rev. A 103 043705] (https://doi.org/10.1103/PhysRevA.103.043705)
209. [Alqedra M K et al 2023 Optical coherence properties of Kramers' rare-earth ions at the nanoscale for quantum applications Phys. Rev. B 108 075107] (https://doi.org/10.1103/PhysRevB.108.075107)

March Meeting 2022 p id.T34.003] (https://meetings.aps.org/Meeting/MAR22/Session/T34.3)

211. [Wade A C J, Mattioli M and Mimer K 2016 Single-atom single-photon coupling facilitated by atomic-ensemble dark-state mechanisms Phys. Rev. A 94 053830] (https://doi.org/10.1103/PhysRevA.94.053830)
212. [Welte S, Hacker B, Daiss S, Ritter S and Rempe G 2018 Photon-mediated quantum gate between two neutral atoms in an optical cavity Phys. Rev. X 8 011018] (https://doi.org/10.1103/PhysRevX.8.011018)
213. [Gottesman D and Chuang I L 1999 Demonstrating the viability of universal quantum computation using teleportation and single-qubit operations Nature 402 390-3](https://doi.org/10.1038/46503)
214. [Uysal M T, Raha M, Chen S, Phenicie C M, Ourari S, Wang M, Van de Walle C G, Dobrovitski V V and Thompson J D 2023 Coherent control of a nuclear spin via interactions with a rare-earth ion in the solid state PRX Quantum 4 010323] (https://doi.org/10.1103/PRXQuantum.4.010323)
215. [Ruskuc A, Wu C-J, Rochman J, Choi J and Faraon A 2022 Nuclear spin-wave quantum register for a solid-state qubit Nature 602 408-13] (https://doi.org/10.1038/s41586-021-04293-6)
216. [Deutsch D, Ekert A, Jozsa R, Macchiavello C, Popescu S and Sanpera A 1996 Quantum privacy amplification and the security of quantum cryptography over noisy channels Phys. Rev. Lett. 77 2818-21] (https://doi.org/10.1103/PhysRevLett.77.2818)
217. [Dur W, Briegel H-J, Cirac J I and Zoller P 1999 Quantum repeaters based on entanglement purification Phys. Rev. A 59 169-81] (https://doi.org/10.1103/PhysRevA.59.169)
218. [Bratzik S, Abruzzo S, Kampermann H and Bru D 2013 Quantum repeaters and quantum key distribution: the impact of entanglement distillation on the secret key rate Phys. Rev. A 87 062335] (https://doi.org/10.1103/PhysRevA.87.062335)

Quantum 3 123] (https://doi.org/10.22331/q-2019-02-18-123)

220. [Jiang L, Taylor J M, Nemoto K, Munro W J, Van Meter R and Lukin M D 2009 Quantum repeater with encoding Phys. Rev. A 79 032325] (https://doi.org/10.1103/PhysRevA.7
221. [Munro W J, Harrison K A, Stephens A M, Devitt S J and Nemoto K 2010 From quantum multiplexing to high-performance quantum networking Nat. Photon. 4 792-6] (https://doi.org/10.1038/nphoton.201
222. [Rolander A, Kinos A and Walther A 2022 Quantum error correction in the noisy intermediate-scale quantum regime for sequential quantum computing Phys. Rev. A 105 062604] (https://doi.org/10.1103/PhysRevA.1
223. [Gritsch A, Ulanowski A, Pforr J and Reiserer A 2024 Optical single-shot readout of spin qubits in silicon (arXiv:2405.05351 [quant-ph])] (https://arxiv.org/abs/2405.05351)
224. [Raha M, Chen S T, Phenicie C M, Ourari S, Dibos A M and Thompson J D 2020 Optical quantum nondemolition measurement of a single rare earth ion qubit Nat. Commun. 11 1605] (https://doi.org/10.1038/s41467-020-15138-7)
225. [Chou C W, de Riedmatten H, Felinto D, Polyakov S V, van Enk S J and Kimble H J 2005 Measurement-induced entanglement for excitation stored in remote atomic ensembles Nature 438 828-32] (https://doi.org/10.1038/nature04353
226. [Jin J, Slater J A, Saglamyurek E, Sinclair N, George M, Ricken R, Oblak D, Sohler W and Tittel W 2013 Two-photon interference of weak coherent laser pulses recalled from separate solid-state quantum memories Nat. Commun. 4 2386] (https://doi.org/10.1038/ncomms338